



Contamination of urban soils in a historical mining town of northern Chile

D. García¹ · J. Tapia^{1,2} · J. Aguilera¹ · C. Vega¹ · P. Zúñiga¹ · P. Lavin³ · L. Rojas⁴ · J. Valdés⁵

Received: 29 March 2023 / Accepted: 26 January 2024 / Published online: 13 March 2024
© The Author(s) 2024

Abstract

In northern Chile, economic activities related to mining and thermoelectric energy have existed in the city of Tocopilla since the early 1900s and metal concentrations in soils have likely been altered by historic anthropogenic activities. To assess the concentrations of Cu, Zn, Pb, Ni, Co, and Cr in urban soils of Tocopilla, a total of 70 superficial (2 cm) and 70 deep (20 cm) soil samples were collected in 2014. Furthermore, to analyze concentration changes in soils over time, 18 superficial (5 cm) samples were collected in 2020–2021. A numerical evaluation (geoaccumulation index, and enrichment factor), principal component analysis, and spatial distribution approach were applied to infer geogenic and anthropogenic influence on the concentrations of these elements. The main conclusions of this research indicate that urban soils of Tocopilla contain geogenic Cu, Zn, Pb, Ni, Co and Cr. However, elevated concentrations of Cu, Zn, and Pb cannot be attributed to a geogenic origin alone, as a proportion of their enrichment is considered to be anthropogenically sourced. The contamination of anthropogenic elements has been found to be related to historic copper mining and thermoelectric energy production. Furthermore, when compared to other sites globally, median concentrations of Cu (945 mg/kg in 2014 and 823 mg/kg in 2020) and Zn (305 mg/kg in 2014 and 196 mg/kg in 2020) in superficial urban soils are among the highest worldwide. Regarding 2020–2021 sampling, Zn and Pb concentrations have increased, while Cu, Cr, Co, and Ni have remained similar to the 2014 samples.

Keywords Urban soil · Contamination · Copper mining · Thermoelectric energy production · Tocopilla · Enrichment factor · Geoaccumulation index

Introduction

Chile is a country located along the southwestern border of South America (Fig. 1A) and its main economic activity corresponds to copper mining, which nearly accounts for 13% of the national global domestic product (GDP; SERNAGEOMIN 2021). Following Spanish conquest of the national territory, anthropogenic activities were performed without proper care of the environment; it was only until 30 years ago (March 1994) that the first Chilean Environment Law (19,300) was enacted as an initial measure to control environmental pollution (Tapia et al. 2019).

Historical anthropogenic activities performed in Chile have given rise to numerous *environmental sacrifice zones* throughout the country; although it is not a legal denomination, it has been used for years to describe highly contaminated zones (VID and CITRID 2020). These areas are segregated and stigmatized locations in which, despite the economic profits previously obtained, inhabitants live in poverty and do not receive the benefits related to those anthropogenic activities (de Souza

✉ J. Tapia
jtapia02@ucn.cl; pepeline.999@gmail.com

¹ Departamento de Ciencias Geológicas, Facultad de Ingeniería y Ciencias Geológicas, Universidad Católica Del Norte, Antofagasta, Chile

² Centro de Estudio Del Agua Del Desierto, CEITSAZA, Universidad Católica Del Norte, Antofagasta, Chile

³ Departamento de Biotecnología, Facultad de Ciencias del Mar y Recursos Biológicos, Universidad de Antofagasta, 1240300 Antofagasta, Chile

⁴ Departamento de Química, Facultad de Ciencias, Universidad Católica del Norte, Antofagasta, Chile

⁵ Laboratorio de Sedimentología y Paleoambientes, Facultad de Ciencias del Mar y de Recursos Biológicos, Instituto de Ciencias Naturales Alexandre von Humboldt, Universidad de Antofagasta, Antofagasta, Chile

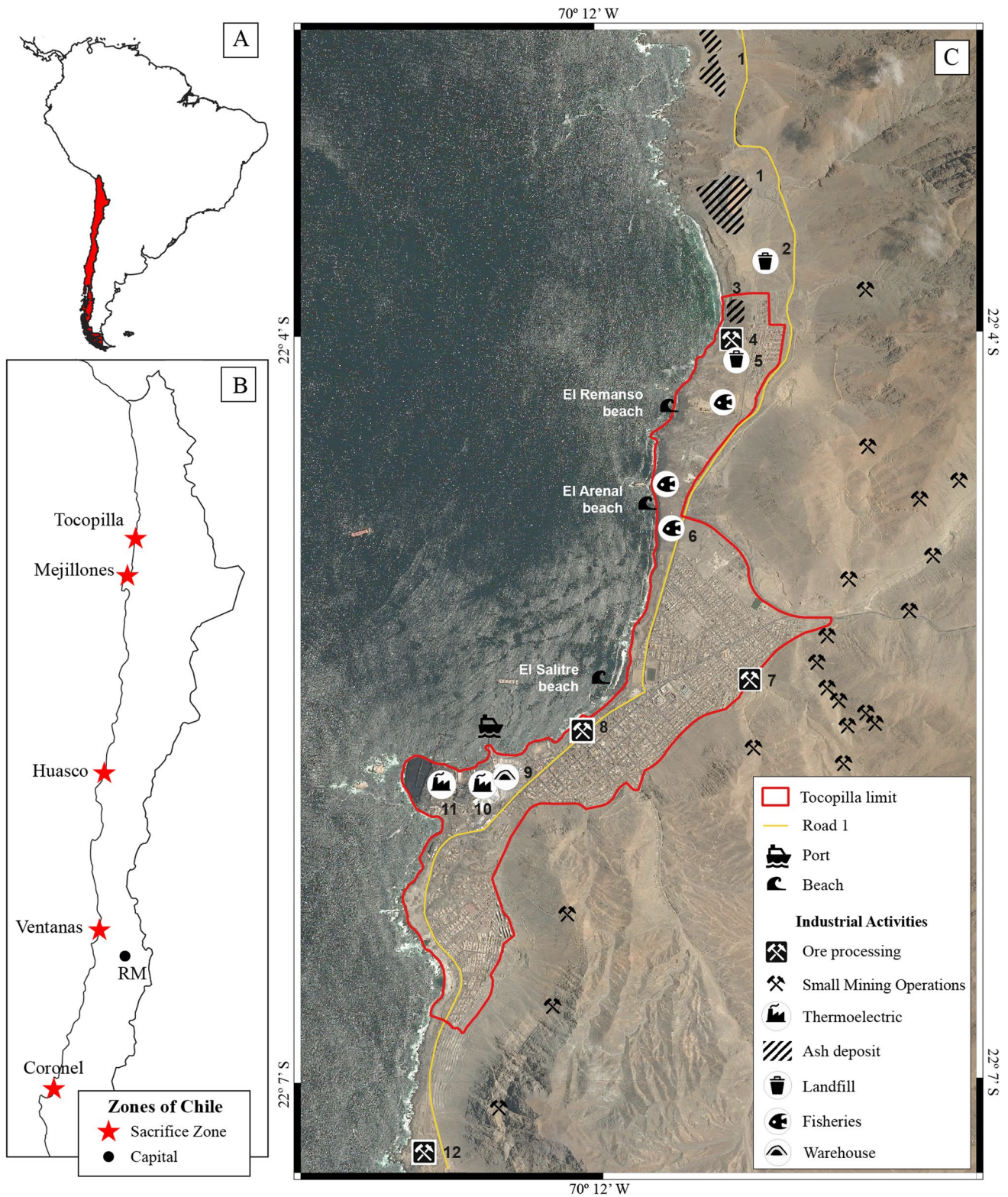


Fig. 1 **A** General location of Chile in South America; **B** Location of the capital city of Chile (RM, Santiago) and sacrifice zones of the country; **C** Industrial activity locations within Tocopilla. Small mining operations are related to operations performed by *pirquineros* (Spanish word referred to people who extract minerals using artisanal techniques). 1. Thermoelectric ash deposits; 2. Ex-Municipal Land-

fill; 3. First ash deposits; 4. Former Cu-processing Plant; 5. Unregistered Landfills; 6. Corpesca S.A.; 7. Tocopilla Benefactor Society (SBT); 8. Tocopilla Mining Company (CMT); 9. SQM potassium warehouse; 10. AES Gener Thermoelectric; 11. Engie S.A. Thermoelectric or CTT; 12. Lipesed Cu-refining company

2021). Known sacrifice zones of Chile correspond to: Coronel in Southern Chile (Tume et al. 2021), Ventanas in Central Chile (Oyarzo-Miranda et al. 2020), Huasco (Pérez et al. 2019) in North-Central Chile, and Mejillones (Gutiérrez et al. 2015) and Tocopilla (Jorquera 2009) in Northern Chile (Fig. 1B).

The assessment of soil quality in Chile is fairly new, however, the following studies have been developed: (i) contaminated and/or industrialized areas such as Arica (Tume et al. 2018c) and Taltal (Reyes et al. 2020) in northern Chile, Talcahuano and Coronel in south-central Chile (Tume et al. 2018a, b, 2021), and also (ii) in schoolyard and playground soils (e.g., Rodríguez-Oroz et al. 2018; Tume et al. 2021; Vega et al. 2022). Despite historic mining activities (Jorquera 2009) and reported health issues (Viviani et al. 2021), the quality of Tocopilla soils has not been fully addressed yet or alleviated. Tocopilla is a coastal town located nearly 1600 km north of Santiago, the capital of Chile (Fig. 1B). This city is inhabited by 25,186 people in a total area of 4039 km² (BCN 2020). Numerous anthropogenic activities are (and were) developed in Tocopilla; the most significant activities correspond to thermoelectric energy production, treatment and refining of copper ores (Lipesed), potassium transportation and storage (SQM), and industrial fisheries (Fig. 1C). Due to these intense current and historic activities, Tocopilla has been declared a particulate matter (PM) saturated zone, exceeding the annual guideline of 50 µg/m³ of breathable 10 µm PM (PM₁₀; BCN 2007; DICTUC 2006). For instance, the average concentration of PM₁₀ ranged between 60.8 and 117 µg/m³ in diverse areas of the city during a 5-week air quality assessment performed in 2006 (DICTUC 2006). Indeed, Tocopilla has shown significant sources of atmospheric pollution (Jorquera 2009) and its inhabitants have been affected by respiratory disease such as asthma and bronchiolitis (Viviani et al. 2021).

Given the historic anthropogenic setting of Tocopilla, a soil sampling campaign was performed in 2014 to obtain a geochemical baseline of potential contaminants related to mining activities (Cu, Zn and Pb) and coal thermoelectric residues (Co, Cr and Ni) in the top (2 cm) and deep (20 cm) portion of the soil. To complement this study and compare the results of 2014, topsoil samples of Tocopilla were obtained in concentric circles around the thermoelectric companies in 2020–2021. The results of both studies are compared and discussed to better understand the environmental issues related to inorganic contaminants in Tocopilla.

Study area

Physiography and geology

The city of Tocopilla resides on the physiographic unit known as the Coastal Plain (Fig. 2A) and above an emerging

marine platform (Quezada et al. 2010). Tocopilla is limited to the east by the Coastal Cordillera (Fig. 2A), a N–S range of 25–45 km width, with elevations ranging between 1 and 2 km. The marine platform is located on the base of the western coastal cliff (~40° W) of the Coastal Cordillera (González et al. 2003; Quezada et al. 2010). Immediately to the east of the Coastal Cordillera, another physiographic feature known as the Central Depression is found (Fig. 2A).

The Coastal Cordillera at the latitude of Tocopilla is constituted by basaltic-andesitic volcanic rocks of Lower to Upper Jurassic age which are intruded by dioritic to granitic magmatic bodies (184–147 Ma). Both the volcanic and intrusive outcrops constitute the Mesozoic basement of this area (López et al. 2018; Fig. 2B). The Mesozoic basement is covered by unconsolidated alluvial and colluvial deposits (González and Niemeyer 2005; Fig. 2B). Tocopilla is located above alluvial and colluvial deposits which cover the Mesozoic basement rocks (Quezada et al. 2010; Fig. 2B).

Regarding mineral ores, this region is associated with the Middle Jurassic to Lower Cretaceous metallogenic belts, which are mainly related to porphyry copper deposits and skarns, iron oxide copper gold (IOCG), and stratabound deposits (Sillitoe 2012, 2003; Fig. 2B).

Climate and hydrometeorological events

Tocopilla is located within an extremely arid zone of northern Chile, and following the Köppen classification, its climate corresponds to a cold desert (BWk; Beck et al. 2018; Kottek et al. 2006). This aridity is produced by: (i) the interaction of regional scale atmospheric systems (such as the South Pacific Anticyclone) related to atmospheric stability, and (ii) the Andes Cordillera, which acts as a barrier that blocks the entry of moisture from the Amazon and Atlantic; both factors inhibit the development of precipitation and facilitate arid conditions (Rutllant et al. 2003; Schulz et al. 2012). Average precipitation of Tocopilla between 01/01/2010 and 11/30/2020 was negligible (0.0046 mm/year) based on data from the National Water Directorate (DGA) of Chile (<https://snia.mop.gob.cl/BNAConsultas/reportes>).

In the area of study, the preferential daily and nightly wind directions are SW (Fig. 2C; 33.8% of the time), and wind speed ranges between 0.5 m s⁻¹ and 2.1 m s⁻¹. No wind conditions represent 3.43% of the day.

Another climatic characteristic of the area is the low elevation fog, known as *camanchaca*. It is a frequent characteristic of the coast, producing a significant relative humidity (~60%; Algoritmos 2019) and low-homogeneous temperatures that range from 12° to 19 °C and 16° to 27 °C in the winter and summer, respectively (Aguas Antofagasta and GHD 2015). The *camanchaca* is halted by the Coastal Cordillera and occasionally is related to

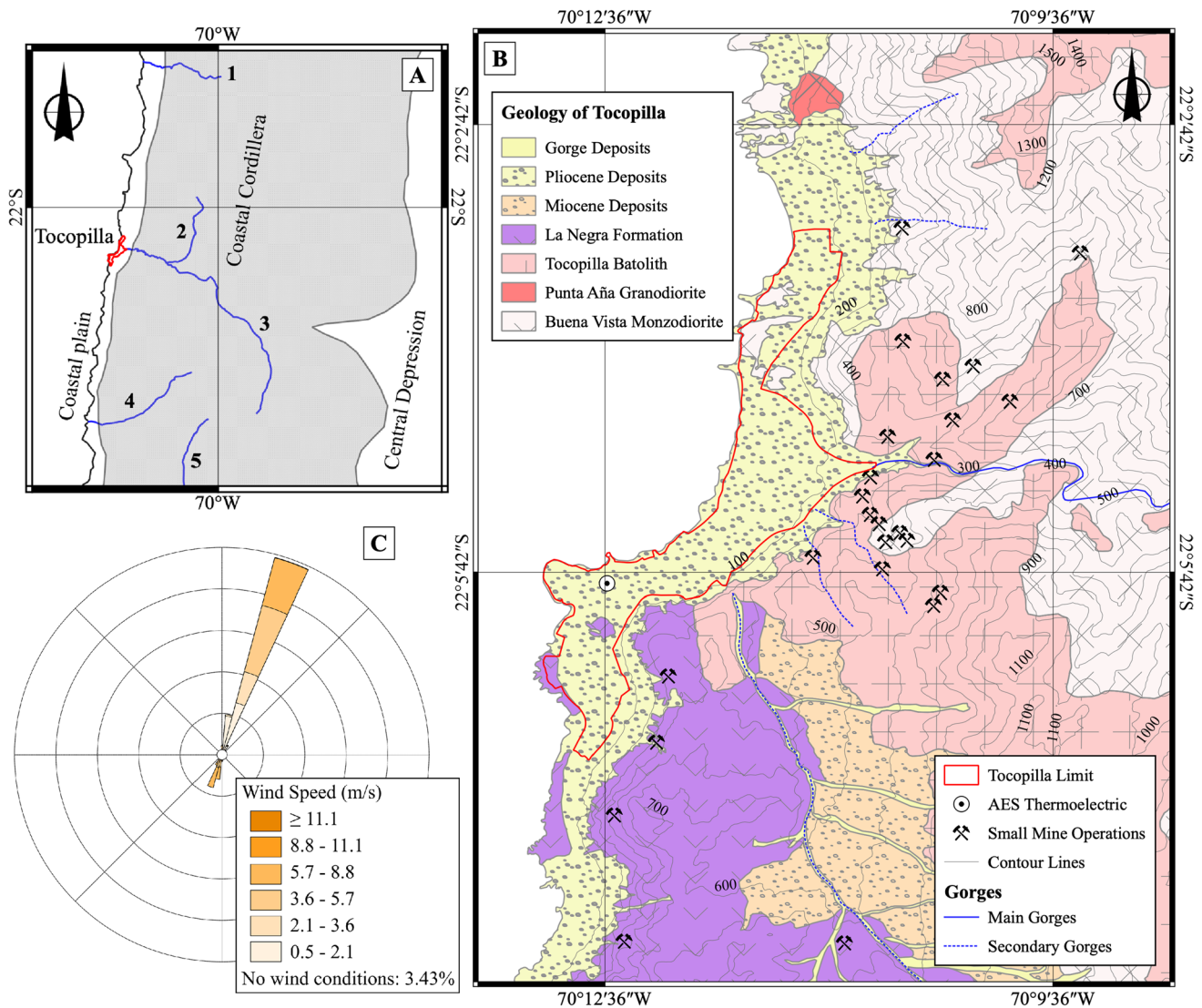


Fig. 2 **A** Physiography at Tocopilla latitude and main gorges; 1. Iquine Gorge; 2. Ancha Gorge; 3. Barril or Seca Gorge; 4. Tres Higueras Gorge; 5. de Tames Gorge. **B** Geology of the study area. **C** Compass rose, which was made using WRPLOT with Cerro Moreno

Station (150 km south of Tocopilla) data from January to June 2021 (<https://climatologia.meteochile.gob.cl/application/historico/datos/Descarga/230>)

low intensity drizzles (Luebert et al. 2007; Rutllant et al. 1998). In addition, the coastal desert of northern Chile is sporadically affected by moderate to strong El Niño Southern Oscillation (ENSO) events that produce short and intense rains (Vargas et al. 2006, 2000). Due to its location and geomorphological features, moderate to heavy rain events are related to massive landslides. Significant debris flow events in Tocopilla have been registered during 1912, 1940, 1991, and 2015 which caused fatalities, damage to the infrastructure, and mining related economic issues (Galaz-Mandakovic 2018).

Hydrogeology and hydrologic systems

The study area is found in the Coastal Basin hydrographic zone along the boundary between Iquine Gorge (992 km²) and Ancha Gorge (1441 km²; Fig. 2A) sub-basins (Muñoz et al. 2014). These sub-basins present a pluvial exoreic regime and drain into the Pacific Ocean, with no evidence of perennial flows, but rather occasional runoff as a result of scarce precipitation (Ferrando 1992).

In the coastal area, rocks have very low permeability and there are no available studies indicating the presence

of a freshwater aquifer in Tocopilla, therefore it has been assumed that this resource is largely absent in the city (DGA 1986). There are some punctual exceptions at 70 and 140 km south of Tocopilla, where evidence indicates the existence of groundwater related to secondary porosity of volcanic rocks (Herrera et al. 2018; Herrera and Custodio 2014). Additionally, the Coastal Cordillera operates as a barrier preventing the groundwater flow to the west; therefore, potential hydrogeologic connections between the Central Depression and the Coastal Cordillera are scarce and occur in areas cut by significant faults at the Loa River outlet (75 km north of Tocopilla), or at Las Vertientes spring in La Negra Gorge (175 km south of Tocopilla; Herrera et al. 2018).

Anthropogenic activities

Numerous anthropogenic activities have been present in Tocopilla during its history, the most significant of which correspond to: mining and ore processing companies, thermoelectric companies, fertilizer companies, and fisheries (Fig. 1C). These activities have been installed within the city, close to schools, health centers, and parks.

Mining activities and ore processing companies. At the beginning of the twentieth century, the Cu concentrate plant and smelter called Tocopilla Benefactor Society (SBT) was operating (Fig. 1C). After its closure around the 1920s, this area was known as “El Escorial” (slag) and it currently operates as a residential zone (Galaz-Mandakovic 2018). In contrast, the Tocopilla Mining Company (CMT; Fig. 1C) started its operations in 1918 on the grounds of a former Cu smelting company and began treating high grade Cu ore. After the installation of a treatment plant in 1960, the CMT abandoned its facility in the urban area of Tocopilla (Fig. 1C). It was inferred from Galaz-Mandakovic (2018) that no remediation efforts were made to clean this area. In 1987, Lipesed S.A. construction started, an ore processing plant 4 km south of Tocopilla (Fig. 1C), and operations began in 1988. After 20 years, Lipesed S.A. finished its operations, and since 2018, the remaining piled material has been transported to another processing plant (30 km south of Tocopilla).

Thermoelectric and energy generation companies. In 1915, the first thermoelectric plant currently known as Central Termoeléctrica Tocopilla (Engie or CTT; Fig. 1C) was installed in the urban area of Tocopilla to supply Chuquicamata, one of the largest and oldest copper deposits exploited in Chile (Galaz-Mandakovic 2021). This facility has used diverse raw materials (oil, bituminous coal, sub-bituminous coal, and petcoke) as fuel over time (Galaz-Mandakovic 2018). It currently produces 268 Mw by coal and 398 Mw by gas. In 1995, the Nueva Tocopilla Thermoelectric plant, currently known as AES Gener (Fig. 1C) began operating (Galaz-Mandakovic 2021); this thermoelectric plant uses coal as a fuel and produces 277 Mw. The ashes

generated from the burning of fuels were deposited to the north of the city (Fig. 1C). In 2022 the CTT stopped using coal and presently its fuel only corresponds to gas.

Fertilizer companies. Since 1988, the SQM company has operated a potassium warehouse (Fig. 1C) intended for the distribution of fertilizers and storage of potassium sulfate and potassium salts, which at least until 2008 were stored in open areas (Jorquera 2009).

Fisheries. In 1959, the extractive activities of the Chilean fishery company known as Corpesca S.A. started (www.corpesca.cl; Fig. 1C). This company processed fish to produce fishmeal and fish oil. In 2012 the company closed its operations in Tocopilla (Galaz-Mandakovic 2018); currently the fisheries are only artisanal.

The historic and current anthropogenic activities of Tocopilla, which mainly include thermoelectric plants and mining companies, might be related to the presence of significant amounts of breathable PM₁₀, exceeding for three consecutive years the annual guideline of 50 µg/m³ (BCN 2007). Considering this pollutant, the city was declared a PM₁₀ saturated zone in 2007 (BCN 2007).

Work methodology

Sampling

Two sampling campaigns were performed in the soils of Tocopilla, one in 2014 and the other in 2020–2021 (Fig. 3A). A total of 88 superficial samples and 70 deep samples were taken, which were divided into 10 baseline superficial and deep samples in 2014 (Fig. 3B, C), 60 superficial and deep samples in 2014 (Fig. 3B), and 18 superficial samples in 2020–2021 (Fig. 3D). For clarity and simplification purposes, throughout the text the superficial sampling of 2014 is called S-2014, the deep sampling of 2014 is called D-2014, and the superficial sampling of 2020–2021 is called S-2020.

The 2014 sampling campaign was exploratory and was performed between July and November 2014 in the upper 2 cm or superficial (S-2014; Supplementary Material 1A) and 20 cm deep (D-2014; Supplementary Material 1B) soils of Tocopilla. During this sampling campaign, 10 superficial and 10 deep soil samples representing the geology of supposedly unimpacted soils, were collected to the north (Fig. 3B) and south (Fig. 3C) of Tocopilla. These samples were obtained in areas protected from the wind to avoid anthropogenic influence coming from Tocopilla and were sampled following a N–S transect (Fig. 3A). The samples obtained to the north (8 superficial and 8 deep) represent soils associated with granitic rocks (northern baseline, Fig. 3B), and the ones obtained to the south (2 superficial and 2 deep) represent soils related to andesitic to basaltic volcanic rocks (southern baseline, Fig. 3C). From the city

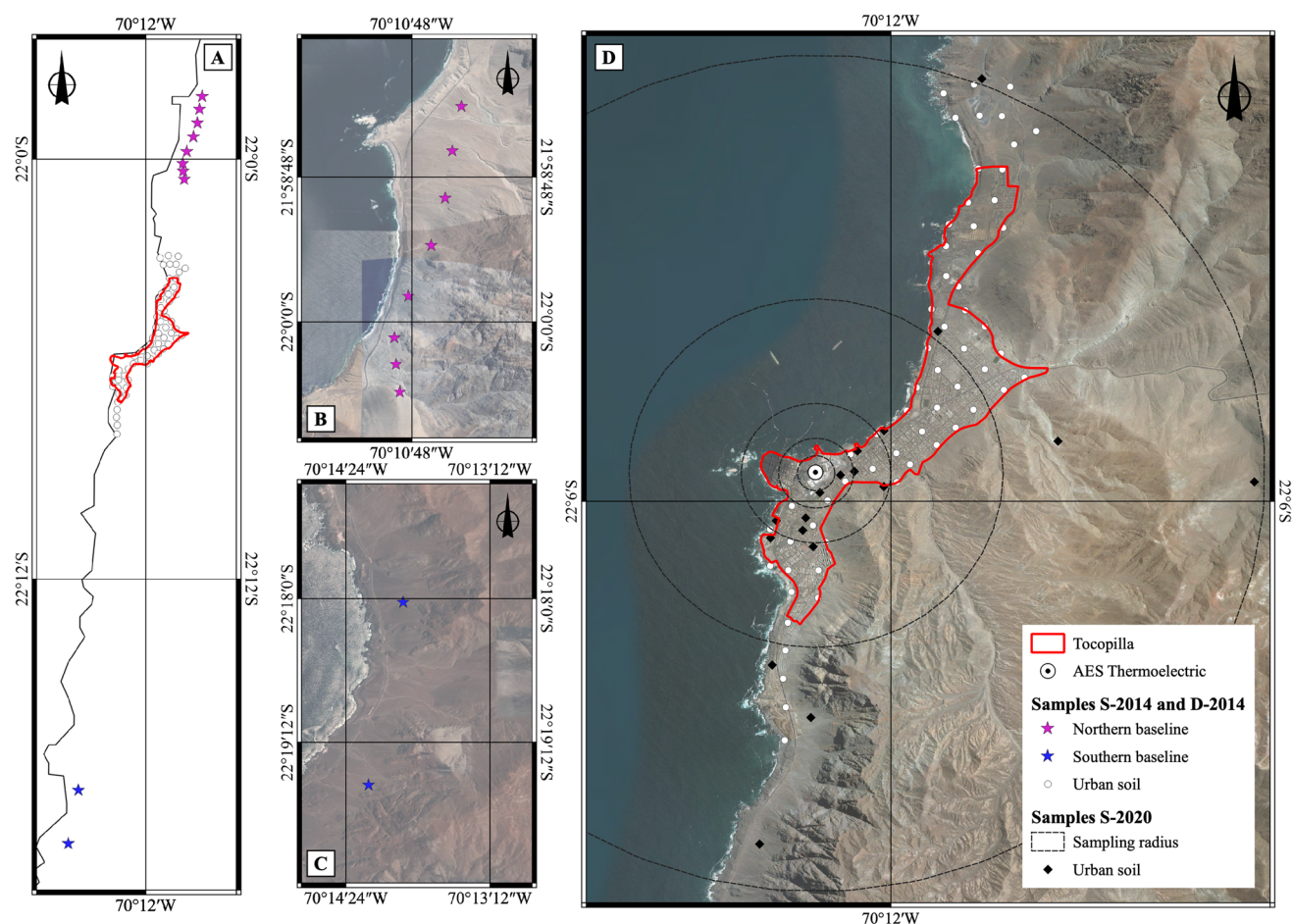


Fig. 3 Sampling sites. **A** General sample locations; **B** Northern baseline samples; **C** Southern baseline samples; **D** Urban Tocopilla sampling sites of 2014 (S-2014 and D-2014) and 2020 (S-2020)

of Tocopilla, 60 superficial and 60 deep samples were collected (Fig. 3D). These samples were obtained from a random point on a 1 m² surface, from a 400 m × 400 m regular grid (Fig. 3D). These samples were collected using previously acid-cleansed plastic shovels. Nearly 1 kg of soil was obtained for each sample and was stored in plastic bags until analysis.

The S-2020 sampling campaign was carried out between November 2020 and April 2021. Due to the fact that during the 2014 sampling campaign it was observed that Tocopilla soils were relatively homogeneous in the upper 10 cm, the upper 5 cm were selected for sampling during the S-2020 campaign (Supplementary Material 1C). A total of 18 samples were taken at an approximate radius of 250 m, 500 m, 750 m, 1000 m, 2500 m, and 5000 m from the AES Gener Thermoelectric plant, as the central point of the sampling circumferences (Fig. 3D). The central point was chosen because this thermoelectric plant was associated with significant concentrations of Cu (between 1025 and 1401 mg/kg) and Zn (between 406 and 653 mg/kg) in the 2014 sampling

campaign. For each radius, samples were taken in the north, east, and south cardinal points (Fig. 3D), where nearly 1 kg of soil samples were collected using a previously acid-cleansed plastic shovel or stainless-steel shovel (depending on the hardness of the soil). Each sample represented a composite of 3 vertices of an equilateral triangle within an area corresponding to 2 m in diameter, at each vertex 300 to 400 g of sample were taken from the uppermost 5 cm of the urban soil.

Physicochemical characteristics of soils

In-situ soil properties

For the S-2020 sampling campaign, pH, temperature, conductivity, and oxidation–reduction potential were measured for each soil sample. These parameters were quantified in a soil sample diluted in distilled water (1 soil: 1 water) using a field multiparameter (HANNA HI-98194).

Metal concentrations

Prior to analyses, the composite soil samples were dried, homogenized with an agate mortar, and divided into two portions using a stainless-steel sample cutter. For the S-2014 and D-2014 sampling campaign, the wet soil samples were dried using an oven at 60 °C and were sieved to a size lower than 75 µm applying a shaker and stainless-steel sieve, following the protocols of the Chilean National Survey of Geology and Mining (Lacassie et al. 2014). For the S-2020 sampling, the wet soil samples were dried using an oven at 50 °C and were sieved to a size less than 63 µm using a shaker and stainless-steel sieve. The decrease in drying temperature was made to avoid changes in the composition of organic matter (OM), although in the Atacama Desert, the maximum accumulation of OM occurs between 40 and 150 cm depth (Mörchen et al. 2019) which is below the sampling depth. This implies that no significant changes in the soil composition should be observed. The change in sieving size was done to consider the potential contaminants related to the clay-silt size, which tends to concentrate metallic contaminants (Zhang et al. 2013).

The soils obtained during the S-2014, D-2014, and S-2020 sampling campaigns were digested using reverse aqua regia i.e., 4 mL HCl + 12 mL HNO₃ + 300 mg of soil sample. These digestions were performed using a hot plate at 100 °C for 1 h in the CEITSAZA Laboratory at Universidad Católica del Norte (UCN). The digested residue was quantified for cobalt (Co), chromium (Cr), nickel (Ni), copper (Cu), zinc (Zn), and lead (Pb). In addition, iron (Fe) was analyzed to normalize other element concentrations. The quantification was done using a Perkin Elmer OPTIMA 7000 DV ICP-OES at the CEITSAZA Laboratory. Quality control (QC) and quality assurance (QA) of the instrument were checked by blanks and calibration curves obtained using a multielement solution measured over the analytical time. To study the QA/QC of the analyses, 23% of the total samples were analyzed in duplicates to check precision, and a certified soil material (ERM-CC141) was run every 25 samples to check accuracy. The detection (DL) and quantification (QL) limits were obtained according to the IUPAC recommendations (Danzer and Currie 1998). All of the studied elements presented a good repeatability calculated between the sample and the duplicate ($R^2 \geq 0.98$; Supplementary Material 2), in addition, the analyses of the certified material were in general within 10% when values were above the quantification limit (Table 1). One exception was the low recovery of Cu from the certified material likely due to the acid reagents used for the digestion. Previous reports indicated that the partial digestion of Cu is related to the incomplete breakdown of oxides, silicates or phosphates to which Cu could be bound (Lo and Sakamoto 2005).

Table 1 Element detection limit (DL), quantification limit (QL), duplicate correlations (DC), certified values (CV) obtained in this study, and certified values (ERM-CC141)

	DL mg/kg	QL mg/kg	DC	Obtained CV mg/kg	CV mg/kg
Cr	2.08	6.33	0.9907 ± 0.0565	26 ± 2.8	31 ± 4
Fe	0.51	1.56	0.9925 ± 0.0387	5977 ± 999	– ± –
Co	0.68	2.07	0.9958 ± 0.0510	8.8 ± 0.7	7.9 ± 0.9
Ni	2.57	7.82	0.9966 ± 0.0390	21.0 ± 2.8	21.9 ± 1.6
Cu	0.67	2.03	0.9997 ± 0.0448	8.2 ± 0.7	12.4 ± 0.9
Zn	1.66	5.06	0.9964 ± 0.0510	56 ± 11	50 ± 4
Pb	1.82	5.54	0.9996 ± 0.0591	26.4 ± 5.4	32.2 ± 1.4

Statistics

The univariate statistics and numerical indices were calculated with the raw data (Supplementary Material 1). To obtain principal component analyses and interpolation maps the values below the detection limit were recalculated as the DL divided by 2 (e.g., Tapia et al. 2018a).

Basic statistics

Basic statistics such as mean, absolute and relative standard deviation, median, median absolute deviation (MAD), minimum, maximum, and percentiles (5, 25, 50, 75, and 95) were calculated. For graphic visualization of certain statistical values, histograms and boxplots were made using OriginPro 2021. For boxplots, the concentrations 1.5 times higher than the third quartile were considered outliers (e.g., Aggarwal 2017).

Element correlations were obtained using the Spearman correlation coefficient (r), which gives more robust results than Pearson when datasets exhibit outliers (Spearman 1961; Zimmerman and Williams 1997). The correlations significance was addressed considering the following absolute values: very high ($r > 0.8$); high ($0.6 < r \leq 0.8$); moderate ($0.4 < r \leq 0.6$), and low ($r \leq 0.4$; Williams 1986).

Principal component analysis

The principal component analysis (PCA) is a statistical multivariate method aiming at explaining most of the variance of a dataset with the minimum number of correlated variables (Anderson 2003). In this study, the PCA was used to identify correlated groups of elements. Since the data distribution presents positive asymmetries, before the PCA analysis, the concentrations were transformed using the centered log ratio (clr ; Eq. 1; Bern et al. 2019; Reimann et al. 2011); due

to the fact that the *clr* transformation is a less subjective method when compared to other log-transformations (Bern et al. 2019; Reimann et al. 2011).

$$clr(x) = \log\left(\frac{x}{g(x)}\right) \quad (1)$$

In this transformation x represents the concentration of the element in the sample and $g(x)$ represents the geometric mean of the dataset; for this transformation all the concentrations must be in the same unit (Bern et al. 2019). The PCA was carried out with standardized variables and varimax rotation (e.g. Mishra et al. 2019; Zhu et al. 2020). For the test determination of the suitability of PCA, the Kaiser–Mayer–Olkin (KMO) test and Bartlett sphericity test were performed. For PCA appropriateness, KMO test must be greater than 0.5, while significance level must be < 0.05 for Bartlett's test (Vural and Cicek 2022).

Spatial and numerical analysis

Shallow versus deep soil

Trace metals are naturally contained in soils by rock weathering. Nevertheless, trace metals derived from anthropogenic activities tend to accumulate in the topsoil (Desaules 2012). The difference of concentration in different soil horizons have been studied in the past by the United States Geological Survey-USGS (Smith et al. 2014). The rate between superficial and deep soil horizons might aid in the constraining of anthropogenic and geogenic sourced elements, because it is assumed that metals of anthropogenic origin are deposited and accumulated mostly on the soil surface (e.g., Chiprés et al. 2009; Desaules 2012).

In this study, a rate between the concentration of the studied elements in superficial soil versus deep soil was performed (S-2014/D-2014). Following McIlwaine et al. (2017), rates above 1.5 were considered to present significant anthropogenic influence. Box-plots and interpolations (see the section "Distribution and interpolation maps") were performed to visualize the rates of each element.

Distribution and interpolation maps

Distribution maps were made using the Geostatistical Analyst extension of ESRI ArcMap 10.8.2 to visualize spatial variations in the elemental concentrations.

Due to a regular grid, interpolation maps using ordinary kriging were applied to the S-2014 and D-2014 datasets. In addition, interpolation maps using the values obtained between the ratio S-2014/D-2014 were performed. Before the interpolation, the concentrations were transformed using *clr* (Eq. 1). The *clr* transformation underestimated the most

extreme outliers. For the S-2014 and D-2014 datasets, a natural break (Jenks) classification was used in the map legends.

Due to the concentric grid, no interpolations were made for the S-2020 dataset and metal concentrations are shown as crosses in the maps. To compare both samplings, classification limits shown in the maps are the same for the S-2014 and S-2020 datasets.

Numerical analysis

To infer the degree of contamination and the metal enrichment in the soils of Tocopilla the geoaccumulation index (I_{geo} ; Muller 1979) and enrichment factor (EF; Zoller et al. 1974; Eq. 3) were calculated. The geoaccumulation index was calculated following Eq. 2.

$$I_{geo} = \log_2 \frac{C_n}{1.5 \times B_n} \quad (2)$$

C_n represents the concentration of the studied element in the sample and B_n corresponds to the concentration of the same element in a background material; a factor of 1.5 is applied to consider the lithological variability (Muller 1979; Nowrouzi and Pourkhabbaz 2014). Müller (1979) defined seven classes of geoaccumulation index ranging from class 0 ($I_{geo} = 0$, unpolluted) to class 6 ($I_{geo} > 5$, extremely polluted). The highest class (class 6) reflects at least a 100-fold enrichment factor above background values.

To calculate the enrichment factor, Eq. 3 was used.

$$EF = \frac{M_m}{(Fe, Al, Ti)_m} / \frac{M_b}{(Fe, Al, Ti)_b} \quad (3)$$

M_m corresponds to the concentration of the element studied in the sample, $(Fe, Al, Ti)_m$ is the concentration of Fe, Al, or Ti in the sample, and M_b and $(Fe, Al, Ti)_b$ correspond to the concentration of the element and Fe, Al, or Ti in the selected background material. For this index, values close to 1 indicate no enrichment and that the soil was probably derived from the background material used for the calculation. Values of $EF > 1.5$ indicate that a significant portion of metal was not delivered from natural weathering processes, rather by other sources. On the other hand, EFs greater than 1 indicate that metals are enriched in the soil surface either from geogenic or anthropogenic sources (e.g. Nolting et al. 1999). These factors were categorized as follows: $EF < 1$ indicates no enrichment; $EF < 3$ indicates minor enrichment; $EF = 3-5$ indicates moderate enrichment; EF between 5 and 10 corresponds to moderately severe enrichment; EF between 10 and 25 indicates severe enrichment; EF values ranging from 25 to 50 are related to very severe enrichment; and EF above 50 is considered extremely severe enrichment (Chen et al. 2007 and references therein).

Table 3 General characteristics of Tocopilla soils

	pH	Eh (V)	Conductivity (mS/cm ⁻¹)	Silt-clay (%)	Sand (%)	Gravel (%)
Mean	7.28	0.184	55	4.5	66.9	28.6
σ	0.65	0.059	36	3.5	10.1	8.5
σ (%)	8.9	32	64	80	15	30
Median	7.39	0.170	44	2.8	65.4	28.5
Range	5.36–7.96	0.113–0.324	6–144	0.8–11.1	52.2–85.6	13.6–45.6
Instrumental accuracy	±0.02	±0.001	±0.001	–	–	–

Table 4 Summary of main univariate statistical parameters of Tocopilla soils

Element	Dataset	<i>n</i>	Mean mg/kg	σ mg/kg	σ %	Minimum mg/kg	P0.05 mg/kg	P0.25 mg/kg	Median mg/kg	P0.50 mg/kg	P0.75 mg/kg	P0.95 mg/kg	Maximum mg/kg	MAD1 mg/kg	MAD2 mg/kg
Cr	S-2020	18	37	18	48	20	21	25	32		46	72	87	13	6.9
	S-2014	60	35	61	174	2.1	5.5	19	25		33	69	484	21	6.8
	D-2014	60	24	16	66	5.6	6.7	14	21		29	59	98	11	6.6
Co	S-2020	18	12	6	53	4.8	5.7	6.7	10		17	22	28	5.1	3.6
	S-2014	60	13	19	147	1.6	2.6	5.5	8.1		15	37	145	8.9	4.0
	D-2014	60	16	10	61	0.7	6.2	11	14		17	37	60	6.1	3.4
Ni	S-2020	18	26	15	59	10	12	15	18		40	52	63	13	4.2
	S-2014	60	25	23	90	2.7	5.1	10	18		35	66	125	16	8.9
	D-2014	60	18	11	61	4.7	6.1	13	16		19	32	72	6.4	3.2
Cu	S-2020	18	2141	3537	165	297	391	612	823		1868	6573	15,212	2143	386
	S-2014	60	1969	3010	153	46	152	517	945		1382	11,480	12,315	1926	423
	D-2014	60	1457	2282	157	16	72	280	555		1462	8656	9748	1499	335
Zn	S-2020	18	544	647	119	54	70	85	196		968	1932	2092	512	130
	S-2014	60	406	509	126	13	20	82	305		486	1781	2942	305	216
	D-2014	60	295	746	253	1.7	5	23	65		203	1235	4600	359	56
Pb	S-2020	18	61	61	100	5.4	11	18	27		115	163	205	51	15
	S-2014	55	23	31	136	2.3	2.6	5.0	10		32	99	174	13	7.0
	D-2014	43	42	82	193	2.3	2.8	6.4	14		38	160	503	44	11

P0.05, P0.25, P0.50, P0.75, and P0.95 correspond to the percentiles 5, 25, 50 or median, 75, and 95

MAD1 absolute standard deviation, MAD2 median absolute deviation

concentrations during the sampling times and at different depths, while Pb, Zn, and to a lesser extent Cu show significant differences (Fig. 4). Average Pb concentrations for S-2020 are nearly three times higher than S-2014 and D-2014, whereas the average concentrations of superficial Zn and Cu (S-2014 and S-2020) exceed that of the deep soil (D-2014) where Zn concentrations are nearly double.

For all of the studied elements and sampling campaigns, histograms show positive asymmetries (Fig. 4). Outlier values are more abundant in S-2014 and D-2014, and Cu and Cr exhibit outlier values in S-2020 (Fig. 4).

Bivariate and multivariate statistics

Spearman correlation coefficient

The Spearman correlation coefficients obtained for the studied metals in S-2014, D-2014, and S-2020 datasets are shown in Table 5. The S-2014 dataset shows a moderate correlation between Zn–Cu ($r=0.54$) and a high correlation between Cr–Zn ($r=0.61$). The D-2014 dataset indicates a very high correlation between Zn–Pb ($r=0.84$), and moderate correlations between Cr–Ni ($r=0.59$) and Cu–Zn

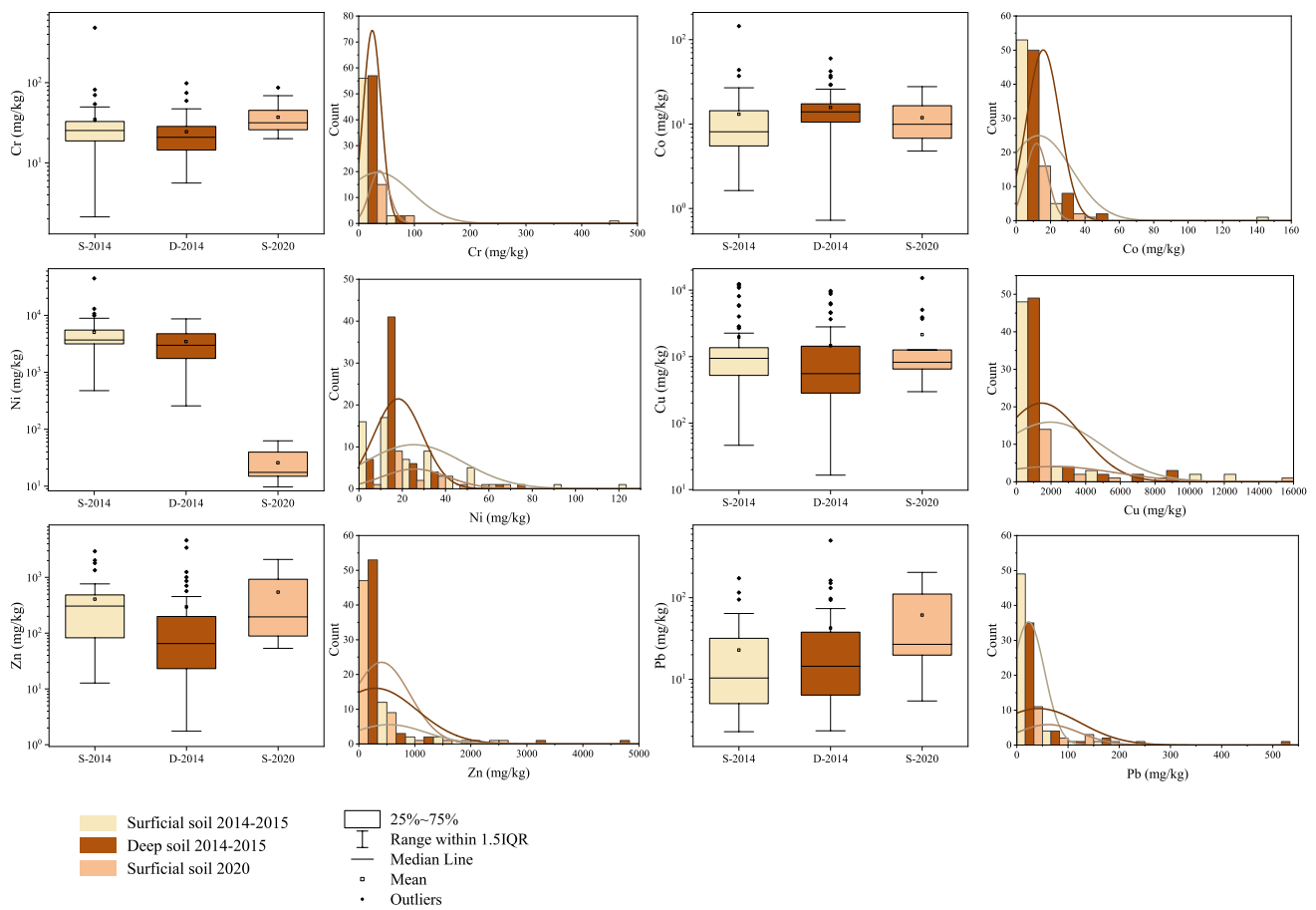


Fig. 4 Box-plots and histograms for the studied metals in surface soil of 2014 (S-2014), 20 cm depth soil of 2014 (D-2014), and surface soil of 2020 (S-2020)

($r=0.52$). As in D-2014, the S-2020 dataset exhibits a very high correlation between Zn–Pb ($r=0.84$), while Cr–Ni and Co–Ni present high correlations ($r=0.65$ and 0.71 , respectively), and Ni–Pb present a moderate negative correlation ($r=-0.53$). Only Pb and Zn (D-2014 and S-2020) present very high (>0.8) correlation coefficients (Table 5).

Principal component analysis (PCA)

The results of the PCA made using rotated component matrix are shown in Table 6. For S-2014 and D-2014, 82% and 83% of the accumulated variance is explained by three principal components (PC1, PC2, and PC3), while for the S-2020, 91% of accumulated variance is explained by three principal components (PC1, PC2, and PC3; Supplementary Material 3). The KMO test is greater than 0.6 for D-2014 and S-2020, and is also higher than 0.5 for S-2014. Furthermore, Barlett’s test of sphericity indicated significance levels <0.001 for all sampling campaigns (Supplementary Material 3).

In the PCA analysis, the following relations were found in the different datasets: (i) S-2014 Zn–Cr and to a lesser extent Cu to PC1, Co–Cu to PC2, and Ni–Pb to PC3; (ii) D-2014 Zn–Pb and to a lesser extent Cu to PC1, Ni–Cr to PC2, and Co–Cu to PC3; and (iii) S-2020 Zn–Pb to PC1, Ni–Cr and to a lesser extent Co to PC2, and Cu–Co to PC3 (Table 6).

Spatial analysis

The interpolated maps obtained for S-2014 and D-2014 datasets present similar patterns for Pb–Cu and lesser for Cr and Zn, these maps show the highest concentrations for Pb, Cu, and Cr in the central and northern areas of Tocopilla. In addition, Cu shows significant concentrations in the southern zone outside of the city in S-2014 (Fig. 5) and D-2014 (up to 9747 mg/kg; Supplementary Material 4). Nickel in the S-2014 dataset shows the highest concentrations in the northernmost and central areas of Tocopilla, whereas in the D-2014 dataset the highest concentrations are found in the downtown portion of the city. For the S-2014 and D-2014 datasets, Co exhibits little variability on its distribution, yet

Table 5 Spearman’s correlation coefficients

	Cr	Co	Ni	Cu	Zn	Pb
A						
Cr	1					
Co	0.28 <i>p</i> =0.030	1				
Ni	-0.08 <i>p</i> =0.569	0.21 <i>p</i> =0.106	1			
Cu	0.39 <i>p</i> =0.002	0.33 <i>p</i> =0.011	-0.08 <i>p</i> =0.550	1		
Zn	0.61 <i>p</i> =0.000	-0.01 <i>p</i> =0.956	-0.38 <i>p</i> =0.003	0.52 <i>p</i> =0.000	1	
Pb	0.47 <i>p</i> =0.000	0.23 <i>p</i> =0.087	0.35 <i>p</i> =0.008	0.24 <i>p</i> =0.075	0.28 <i>p</i> =0.041	1
B						
Cr	1					
Co	0.32 <i>p</i> =0.012	1				
Ni	0.59 <i>p</i> =0.000	0.43 <i>p</i> =0.001	1			
Cu	0.14 <i>p</i> =0.275	0.44 <i>p</i> =0.001	0.12 <i>p</i> =0.365	1		
Zn	0.36 <i>p</i> =0.0053	0.24 <i>p</i> =0.064	0.31 <i>p</i> =0.016	0.52 <i>p</i> =0.000	1	
Pb	0.39 <i>p</i> =0.009	-0.04 <i>p</i> =0.813	0.29 <i>p</i> =0.056	0.01 <i>p</i> =0.963	0.75 <i>p</i> =0.000	1
C						
Cr	1					
Co	0.43 <i>p</i> =0.078	1				
Ni	0.65 <i>p</i> =0.003	0.71 <i>p</i> =0.00098	1			
Cu	-0.07 <i>p</i> =0.798	0.18 <i>p</i> =0.479	-0.10 <i>p</i> =0.708	1		
Zn	-0.26 <i>p</i> =0.299	-0.31 <i>p</i> =0.208	-0.49 <i>p</i> =0.040	0.43 <i>p</i> =0.072	1	
Pb	-0.40 <i>p</i> =0.101	-0.41 <i>p</i> =0.093	-0.53 <i>p</i> =0.023	0.49 <i>p</i> =0.038	0.84 <i>p</i> =0.000	1

A Superficial sampling campaign 2014 (S-2014), B Deep sampling campaign 2014 (D-2014); C Superficial sampling campaign 2020 (S-2020)

Table 6 Rotated component matrix for different sampling campaigns

	S-2014				D-2014				S-2020		
	Component 1	Component 2	Component 3		Component 1	Component 2	Component 3		Component 1	Component 2	Component 3
Cr	0.80	0.17	0.25	Cr	0.28	0.81	0.06	Cr	-0.13	0.96	-0.06
Co	0.03	0.92	0.19	Co	-0.01	0.25	0.92	Co	-0.43	0.43	0.72
Ni	-0.18	0.24	0.84	Ni	0.13	0.88	0.19	Ni	-0.46	0.76	0.25
Cu	0.55	0.71	0.02	Cu	0.66	-0.06	0.61	Cu	0.36	-0.12	0.87
Zn	0.94	0.09	-0.10	Zn	0.87	0.24	0.05	Zn	0.95	-0.13	0.09
Pb	0.36	0.004	0.78	Pb	0.86	0.30	-0.001	Pb	0.84	-0.42	0.07

For each dataset, the three principal components are shown

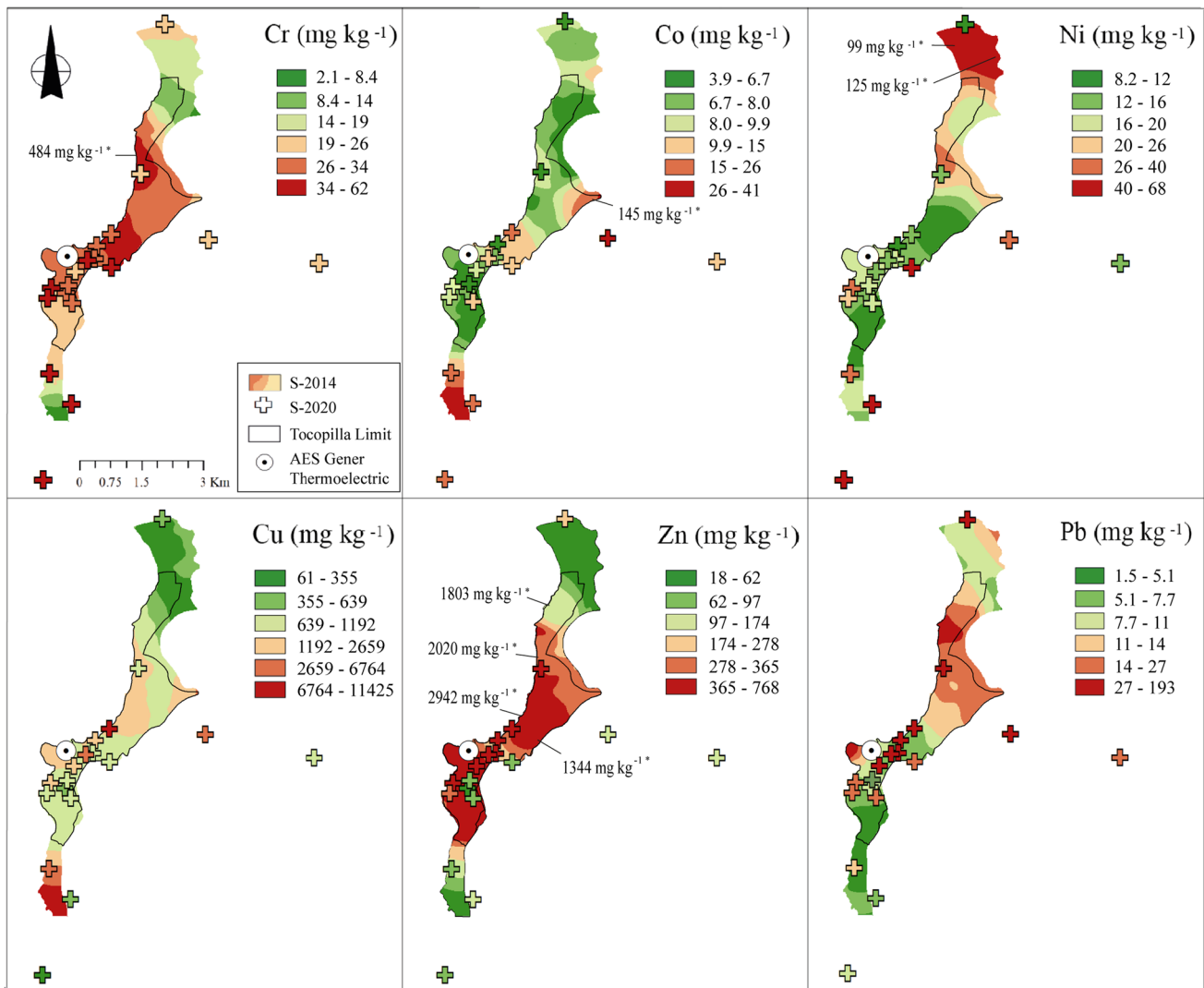


Fig. 5 Spatial distribution of metals in superficial soils of Tocopilla. Chromium (Cr); cobalt (Co); nickel (Ni); copper (Cu); zinc (Zn); lead (Pb). S-2014 concentrations are represented by interpolation using

ordinary kriging. S-2020 concentrations are represented by crosses. Legend applies to both sampling campaigns. *Outliers concentrations in S-2014 were underestimated by ordinary kriging

the southern and central (near AES Thermoelectric) areas show the highest values for S-2014 and D-2014, respectively. The distribution of S-2020 dataset is similar to S-2014 for Cu, Cr, Ni, and Co (Fig. 5); nevertheless, Ni and Cr concentrations are significantly higher in southern Tocopilla, while Pb concentrations are higher in close proximity to the port compared to 2014 (Fig. 5 and Supplementary Material 4).

The ratio between S-2014/D-2014 was interpolated (Fig. 6). Most of the elements present higher superficial concentrations of soils when compared to the deep soils (Fig. 6). Of the studied elements, Co, Cr, and Ni show most of their rates below 1.5; Cu and Pb exhibit nearly half of their values above this rate, while Zn presents most of its rates above 1.5. High S-2014/D-2014 ratios of Cu were observed in the southern area of Tocopilla, while the highest ratios of Pb

were observed in the northern and southern limits of the sampling area, whereas Ni showed higher rates in the northern area of the city (Fig. 6).

Geoaccumulation index and enrichment factor

Table 7A shows the results of I_{geo} calculated with different background materials. The elements Cu, Pb, and Zn show higher values of I_{geo} when compared to Ni, Cr, and Co. In fact, the latter elements were generally classified as non-soil contaminants. For Cu, Pb, and Zn, I_{geo} shows a significant variability depending on the background material used and can change from non-contaminant to strong contaminant (Table 7A). The D-2014 and S-2014 datasets show a similar contamination degree, although Cu and Zn exhibit lower

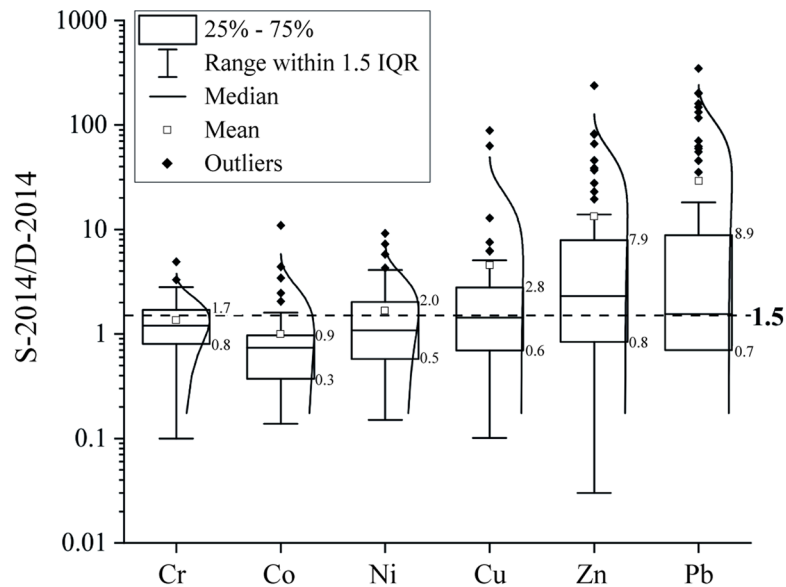
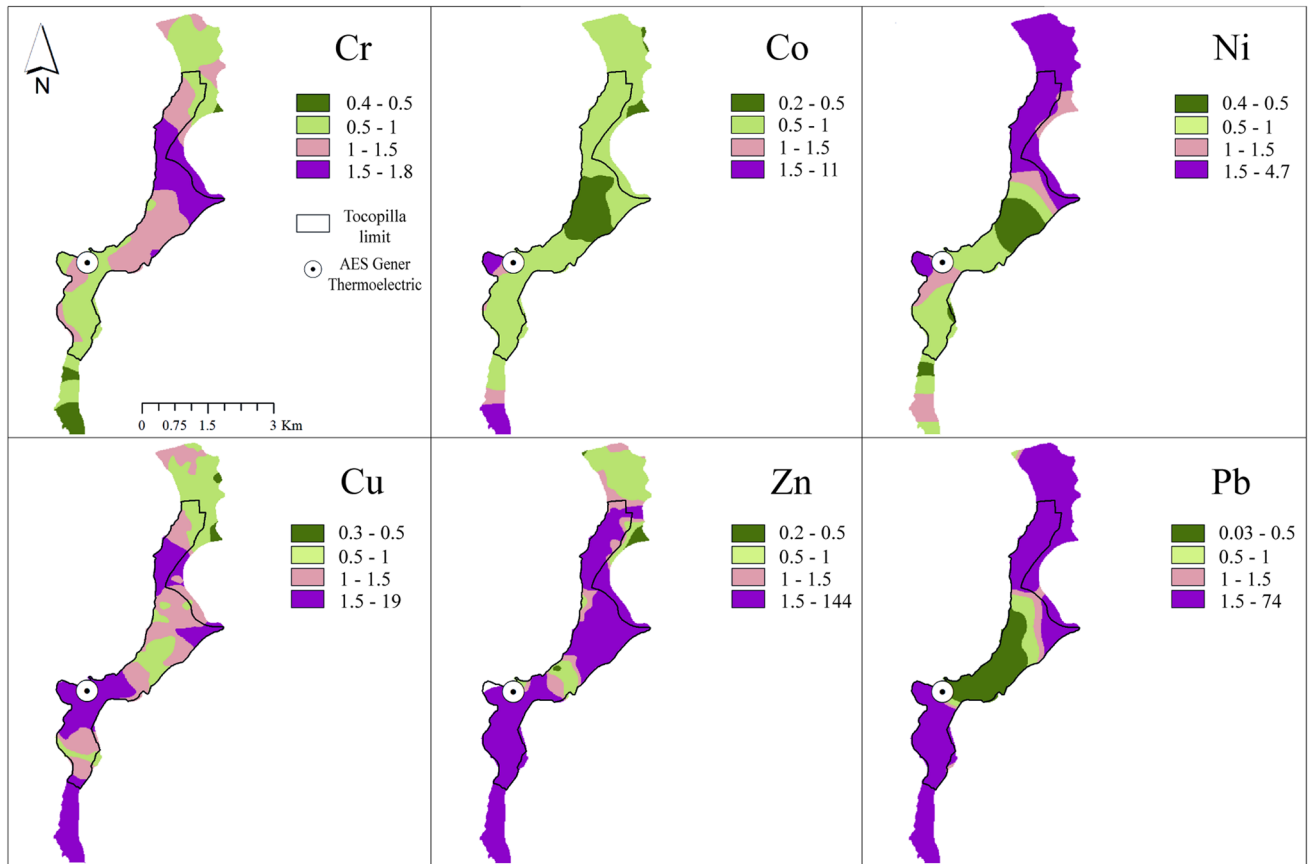


Fig. 6 Top: Interpolation of S-2014/D-2014 using ordinary kriging. Chromium (Cr); cobalt (Co); nickel (Ni); copper (Cu); zinc (Zn); lead (Pb). Bottom: Boxplots showing the rate between the concentration of superficial soil (S-2014) and deep soil (D-2014). The dotted line

shows the 1.5 value, which has been proposed as the limit of anthropogenic influence (McIlwaine et al. 2017); the straight lines represent the normal distribution of each element

Table 7 (A) Average Geoaccumulation Index (I_{geo}) calculated with different background materials. (B) Average Enrichment Factor (EF) calculated using different background materials

Dataset	Background material	(A) I_{geo}						(B) EF					
		Cr	Co	Ni	Cu	Zn	Pb	Cr	Co	Ni	Cu	Zn	Pb
S-2200	Northern baseline ^a	0.17	-0.76	-1.26	0.45	1.66	1.11	1.95	0.83	0.70	2.14	4.39	3.07
	Southern baseline ^a	-0.04	-1.53	-0.57	0.07	-0.52	0.74	2.10	0.61	1.40	2.03	1.20	2.95
	Volcanic rocks ^b	-1.54	-1.97	-0.85	1.70	-0.18	1.60	2.35	1.41	3.65	19.90	4.79	16.87
	Volcanic rocks ^c	-0.31	-	0.37	-	-	-	6.37	-	9.85	-	-	-
	Intrusive rocks ^b	-2.34	-1.97	-1.26	4.64	1.80	2.39	1.28	1.34	2.60	145.29	17.95	27.82
	Intrusive rocks ^c	-1.89	-	-0.26	-	-	-	1.54	-	4.58	-	-	-
	UCC ^d	-2.13	-1.36	-2.01	4.29	2.21	0.07	0.87	1.21	0.91	67.12	14.08	3.27
	UCC ^e	-1.80	-1.18	-1.54	4.35	0.74	-	-	-	-	-	-	-
	Average	-1.23	-1.46	-0.92	2.58	0.95	1.18	2.35	1.08	3.38	47.30	8.48	10.80
Median	-1.67	-1.45	-1.06	3.00	1.20	1.11	1.95	1.21	2.60	19.90	4.79	3.27	
S-2014	Northern baseline ^a	-0.15	-1.05	-1.24	0.65	2.37	-0.25	1.07	0.72	0.49	1.57	5.65	1.11
	Southern baseline ^a	-0.36	-1.83	-0.55	0.27	0.18	-0.63	1.15	0.52	0.99	1.50	1.54	1.06
	Volcanic rocks ^b	-1.86	-2.27	-0.83	1.90	0.52	0.23	1.28	1.21	2.59	14.65	6.16	6.09
	Volcanic rocks ^c	-0.63	-	0.40	-	-	-	3.48	-	6.99	-	-	-
	Intrusive rocks ^b	-2.65	-2.27	-1.24	4.84	2.50	1.02	0.70	1.15	1.85	106.97	23.10	10.04
	Intrusive rocks ^c	-2.21	-	-0.24	-	-	-	0.84	-	3.25	-	-	-
	UCC ^d	-2.45	-1.65	-1.99	4.49	2.91	-1.30	0.48	1.04	0.65	49.42	18.11	1.18
	UCC ^e	-2.11	-1.47	-1.52	4.54	1.44	-	-	-	-	-	-	-
	Average	-1.55	-1.76	-0.90	2.78	1.65	-0.18	1.29	0.93	2.40	34.82	10.91	3.89
Median	-1.99	-1.74	-1.03	3.19	1.90	-0.25	1.07	1.04	1.85	14.65	6.16	1.18	
D-2014	Northern baseline ^a	-0.43	-0.27	-1.38	-0.12	0.14	0.14	1.15	1.30	0.61	1.50	1.50	2.06
	Southern baseline ^a	-0.64	-1.05	-0.69	-0.50	-2.05	-0.23	1.24	0.94	1.22	1.43	0.41	1.98
	Volcanic rocks ^b	-2.14	-1.48	-0.96	1.13	-1.71	0.63	1.38	2.20	3.20	13.98	1.64	11.33
	Volcanic rocks ^c	-0.91	-	0.26	-	-	-	3.75	-	8.62	-	-	-
	Intrusive rocks ^b	-2.93	-1.48	-1.38	4.07	0.27	1.42	0.76	2.09	2.28	102.06	6.14	18.68
	Intrusive rocks ^c	-2.49	-	-0.38	-	-	-	0.90	-	4.01	-	-	-
	UCC ^d	-2.73	-0.87	-2.12	3.72	0.69	-0.90	0.51	1.88	0.80	47.15	4.82	2.20
	UCC ^e	-2.40	-0.69	-1.66	3.78	-0.79	-	-	-	-	-	-	-
	Average	-1.83	-0.97	-1.04	2.01	-0.57	0.21	1.38	1.69	2.96	33.22	2.90	7.25
Median	-2.27	-0.96	-1.17	2.43	-0.32	0.14	1.15	1.88	2.28	13.98	1.64	2.20	

The background values applied were obtained from: ^aThis study (the mean value presented in Table 2); ^bOliveros et al. (2007); ^cRogers and Hawkesworth (1989); ^dRudnick and Gao (2003); ^eHu and Gao (2008)

The bold numbers refer to the highest average geoaccumulation index and enrichment factors within the studied elements

and Pb higher values in D-2014. The contamination degree for Cu is similar during 2014 and 2020, whereas Pb and Zn increase their level in 2020 (Table 7A).

A summary of EFs is shown in Table 7B. Iron normalization shows relatively uniform values, which can be associated with fine solid surfaces and to the fact that its geochemistry is similar to that of many trace metals (Bhuiyan et al. 2010). In general, the decreasing order of enrichment obtained for soils of Tocopilla corresponds to: Cu > Pb or Zn > Ni > Cr > Co. Copper is the metal with the highest enrichment in soils for both years and depths, showing moderate to extremely severe enrichment (Table 7B). In general, EFs were lower when using a local baseline (Cu, Pb, Zn and

Ni), and local volcanic rocks show lower indices than local intrusive rocks (Cu, Pb, and Zn).

Discussion

Physicochemical and geochemical environment of Tocopilla soils

The studied soils correspond to *aridisols* which are present under circumneutral pH and oxidizing conditions (Table 3). In addition, they are predominantly constituted by the sand fraction, whereas the clay-silt grain size presents proportions

ranging from 0.8 to 11.1% (Table 3). The dominant grain size implies that the soils of Tocopilla are associated with a low adsorption/absorption and good infiltration capacity (Aprisal et al. 2019). However, *aridisols* are characterized by the accumulation and concentration of soluble and insoluble weathering products (Soil Survey Staff 1999); moreover, some authors indicated that in arid and hyper-arid zones, similar to Tocopilla, soils are a reservoir of chemical components and trace elements (Corradini et al. 2017). This suggests that soils of the area might concentrate and accumulate metals, which could be benefited from the circumneutral pH that prevents metal mobilization (Zhai et al. 2018).

Regarding rock geochemistry of the study area, volcanic and intrusive rocks near Tocopilla are characterized by an andesitic to basaltic composition. The main oxides are present in the following ranges: SiO₂ 51.1 to 56.4%, Al₂O₃, 14.6 to 18.6%, FeO_{tot} 5.2 to 10.3%, MnO 0.1 to 0.3%, MgO 2.97 to 5%, CaO 2.9 to 10.3%, Na₂O 3.3 to 4.8%, K₂O 0.5 to 2.9%, TiO₂ 0.8 to 1.4%, P₂O₅ 0.1 to 0.41% (Oliveros et al. 2007). In relation to trace elements, the Coastal Cordillera of Tocopilla contains important Cu deposits (Sillitoe 2003) which are usually hosted by La Negra Formation (Fig. 2B), and show increased natural concentrations of Cu (up to 348 mg/kg) and other elements such as Zn (up to 186 mg/kg; Oliveros et al. 2007) when compared to the UCC. Based on the spatial distribution of metal concentrations coupled with numerical indices such as I_{geo} and EF, the geochemistry of the studied trace elements was classified into two groups: (i) one related to Ni–Cr–Co, elements with a narrower range of values, lower standard deviations (Table 4), and lower indices (Table 7); and (ii) a second group related to Cu–Pb–Zn, which presents a wide range of concentrations, higher standard deviations (Table 4), and enhanced indices (Table 7). Multivariate statistics (e.g., Ni–Cr in PC2 of D-2014 dataset; Ni–Cr and lesser Co in PC2 of S-2020 dataset; Zn–Pb–Cu in PC1 of D-2014 dataset; Zn–Pb in the PC1 of S-2020 dataset; Table 6) and interpolation maps (Fig. 5) also indicate the existence of two groups in the soils of Tocopilla. The Cu–Pb–Zn group coincides with zones in close proximity to anthropogenic emissions, and the EFs ratio indicates that their concentrations cannot be explained only by the weathering of the rocks present in Tocopilla (Table 7B). The existence of positive outlier values in both groups (Fig. 4) suggests that natural concentrations are probably affected by external sources (Tume et al. 2018b).

Anthropogenic versus geogenic metals in soils of Tocopilla

In relation to the previously described groups, because of their distribution and numerical indices, Ni–Cr–Co and Cu–Pb–Zn were classified as mostly geogenic and anthropogenic in origin, respectively. In addition, the S-2014/D-2014

rate indicated that values elevated above 1.5 were present in the following (decreasing) order: Zn (67%) > Pb (52%) > Cu (48%) > Ni–Cr (37%) > Co (10%). This classification is supported by the fact that the Cu–Pb–Zn group presents nearly half or more than half of their values above 1.5 (McIlwaine et al. 2017).

Geogenically sourced elements (Cr–Co–Ni)

The lowest indices found for Cr, Co, and Ni suggested a general geogenic origin, although in some cases anthropogenic sources cannot be excluded. For instance, the highest values of Cr were found in the central area of Tocopilla (Fig. 5), a zone where mining activities were performed in the 1900s (Galaz-Mandakovic 2018). The highest values of Co are observed in areas where present and past mining operations were found (Fig. 5), which might be explained by relatively enhanced natural concentrations of Co (21–29 mg/kg; Oliveros et al. 2007) in the host rock of treated ores. In the case of Ni, the superficial soil concentration of the northernmost baseline (Fig. 3) is five times higher than deep soils (Table 2) where dominant SW wind directions (Fig. 2C) would allow for the transport of metal-rich material from Tocopilla to sectors far from its emission sources. Positive anomalies of Ni within the city were found in the fly ash deposits in northern Tocopilla (Figs. 1, 5, and 6). From 1983 to 2001, bituminous and subbituminous coal were the main fuel in thermoelectric plants of Tocopilla; subsequently (from 2001 to 2007), coal was replaced by petcoke (Galaz-Mandakovic 2018, 2021). Petcoke has Ni concentrations higher than coal (e.g., Hower et al. 2005; Langmyhr and Aadalen 1980) and this element tends to concentrate in fly ash during the combustion processes (e.g., Álvarez-Ayuso et al. 2006; Ibrahim 2015). Therefore, fly ash produced by petcoke burning might be related to higher Ni content. In addition, a ratio of 0.36 between Ni and V has been observed in PM of the city, which is characteristic of coal and residual oil combustion (Jorquera 2009). Accordingly, and although most of Tocopilla does not present Ni contamination, the Ni-enriched areas are probably related to thermoelectric plant residues and wind transport.

For Cr, Co, and Ni, important changes between the 2014 and 2020 concentrations were not observed (Fig. 4 and Table 4).

Anthropogenically sourced elements (Cu–Zn–Pb)

Copper, Zn, and Pb showed the highest indices and rates suggesting that their enrichment in soils is largely due to anthropogenic sources. Lower indices for these elements were obtained using local volcanics when compared to intrusives as background (Table 7); these lower indices might reflect Cu deposits hosted by volcanics in this zone (Zambra

et al. 2007). Additionally, in the vicinity of Tocopilla, volcanics show enriched concentrations of Cu and Zn when compared to the UCC (Table 2).

Copper is an ubiquitous element of old Chilean mine tailings (Alcalde et al. 2018), which are present in Tocopilla (e.g., CMT). Contamination and enrichment of Cu in the soils of this city was obtained using different background materials (Table 7), suggesting that an important anthropogenic origin exists for this metal. Copper tends to adhere to soil particles better than other trace metals, lowering its mobility and increasing its accumulation in the soil (Alloway 2013). A previous environmental assessment made in particulate matter lower than 10 μm (PM_{10}) and 2.5 μm ($\text{PM}_{2.5}$) of Tocopilla established that the source of Cu in this environmental matrix corresponded to the Lipesed ore Cu processing plant (Fig. 1; Jorquera 2009). However, high Cu concentrations were not observed in the central portion of Tocopilla (as in this study; Fig. 5) which might be explained by the fact that Lipesed was active during the Jorquera (2009) assessment (while downtown emissions were inactive), not favoring the production of PM_{10} and $\text{PM}_{2.5}$. Regarding Cu concentrations between 2014 and 2020, no important changes were observed (Fig. 4 and Table 4), which might be explained by mining activities and the remaining Cu from ancient mining.

In Tocopilla soils, the positive correlation between Zn and Pb (0.28 for S-2014, 0.75 for D-2014, and 0.84 for S-2020; Table 5) indicated a probable common origin. Despite presenting a lower contamination and enrichment degree in soils when compared to Cu, environmental indices for Zn and Pb suggest a significant anthropogenic origin (Table 7). Zinc and Pb concentrations in the central and northern Tocopilla overlapped with the Cu anomalies suggesting a potential relationship of both metals with mining activities (Fig. 5). Potentially toxic metals such as Zn and Pb are normally found in Cu-mine tailings of Chile and their concentrations were higher in historical mine tailings when compared to present time mine tailings (Rubinos et al. 2021). In addition, in the vicinity of mining activities these metals tend to persist in the soils after mine closure (e.g., Khalid et al. 2017; Wang et al. 2014). Both old tailings and metal persistence could explain the enhanced concentrations of Cu, Zn, and Pb nearby CMT at city downtown. Furthermore, significant concentrations of Pb (S-2014 and S-2020) in the northernmost part of the city could be related to fly ash from thermoelectric activities (Fig. 5). A previous study showed that contaminant elements such as Pb are preferably absorbed on the surface of fly ashes (e.g., Sharma and Tripathi 2008). Also, Jorquera (2009) established that coal and oil combustion were a source of Pb in $\text{PM}_{2.5}$ in Tocopilla. Moreover, a significant correlation between Pb (0.78) and Ni (0.84) in PC3 (S-2014; Table 6) might suggest that fly ash contributes to increased Pb concentrations in the

northernmost soils of the study area. Regarding Zn and Pb, the increased levels found in the last sampling was likely associated with the enactment in 2010 of the national law to reduce atmospheric pollution (PM_{10}) in Tocopilla. While the emissions of thermoelectric companies such as AES Gener and Engie S.A. were considered to be the main sources of PM_{10} and they were limited, no measures were applied to specifically control Pb and Zn emissions (BCN 2010). In addition, increased concentrations might be related to the redistribution of these elements during hydrometeorological events that affected this city (e.g., 2015 and 2017 mudslides; see the section "Redistribution of metals in the soils of Tocopilla").

Redistribution of metals in the soils of Tocopilla

Heterogeneous soil profiles exhibit lithologic discontinuities and pedogenic processes that could redistribute metals (Desaules 2012). In Tocopilla, the soils are characterized by scarce to non-existent available humidity, and pedogenetic processes are expected to be minimal (Soil Survey Staff 1999). Nevertheless, in this particular area of the Atacama Desert heavy rains occur associated with ENSO events (Vargas et al. 2000); these hydrometeorological events increase the mobilization of trace elements from arid mountainous areas (such as the Coastal Cordillera, eastern limit of Tocopilla) to populated (flat) zones through debris flow (e.g., Copiapó landslide; Corradini et al. 2017). In Tocopilla, the outlet of gorges located in the central and northern portions of the city are typically affected by landslides (Galaz-Mandakovic 2018), which coincide with the highest concentrations of Pb and Zn in deep soils (Supplementary Material 4). Deep soils distribution might suggest historic debris flow events of Tocopilla were likely responsible of redistribution of soil trace elements content. In this regard, the use of the rate S-2014/D-2014 is not a good indicator of geogenic vs anthropogenic origin. However, S-2014/D-2014 rate may reflect the influence of modern anthropogenic activities on Cu, Pb, and Zn deposition since a ratio ≥ 1.5 (Fig. 6) indicates a significant accumulation in superficial rather than deep soils.

Additionally, metal redistribution occurred in the coastal areas. Most of the historic mining activities were developed on the shores and significant metal contents were found in beach sediments throughout the city (e.g., El Salitre, El Arenal, and El Remanso beaches; Figs. 1 and 6). Between 1960 and 1980, CMT (Fig. 1C) dumped tailings directly into the sea (Galaz-Mandakovic 2018, 2021 and references therein), staining the sands with black tones. Due to this historic contamination, El Salitre Beach (Fig. 1C) cleaning was completed in 2018. The contaminated sand was used to fill a geotube (highly resistant fabric), covered with rock-blocks to make a breakwater and attenuate the waves of this

artificial beach. Despite the fact that the geotube is classified as a resistant material, its weathering may cause damage to marine ecosystems through the slow release of metallic components into the ocean (e.g., Carneiro et al. 2018).

Global comparisons to Tocopilla soils

As observed in the previous sections, the urban soils of Tocopilla were and are affected by anthropogenic contaminants. Table 8 shows different cities around the world where the metal content in soils were studied. In cities with high population density and tourism such as Bangkok (Thailand) and Hong Kong (Lee et al. 2006; Wilcke et al. 1998) in Asia, Galway (Ireland), Palermo, Naples and Salerno (Italy) in Europe (Cicchella et al. 2020; Imperato et al. 2003; Manta et al. 2002; Zhang 2006), or Baltimore (United States) in North America (Yesilonis et al. 2008), high Pb concentration was associated with vehicle transport, which also might contribute to Cu and Zn enrichment (e.g., Galway; Zhang 2006). In Dublin, Ireland, the topsoil Pb concentration was related to diffuse atmospheric emissions from traffic and Pb-rich (UK) coal combustion in homes and industries (Glennon et al. 2014). Despite the fact that leaded gasoline was banned on April 2001 in Chile (Tchernitchin et al. 2006), various industries are close to residential areas and the highway (Ruta 1; Fig. 1) which traverse Tocopilla; thus, both the traffic and close proximity to industrial activities could

explain the increased concentrations of Pb in these urban soils. When comparing Tocopilla urban soils to another northern Chile cities, higher values of Pb were related to the storage of Pb concentrate in the port of Antofagasta (170 km south of Tocopilla; Tapia et al. 2018b) and the storage of hazardous toxic mining waste in Arica (575 km north of Tocopilla; the waste was imported by Promel Chile from the Swedish Boliden Metals); these materials were stored in suburbs of Arica between 1983 and 1985 where later a residential area was built and inhabitants were exposed for more than 10 years (Tchernitchin et al. 2006). Furthermore, in Bangkok, Hong Kong, Oslo (Norway), Naples, and Lisbon (Portugal) significant concentrations of Cu, Pb, and Zn in soils are found near different types of industrial activities (Cachada et al. 2013; Imperato et al. 2003; Lee et al. 2006; Tjihuis et al. 2002; Wilcke et al. 1998). At Tocopilla, Cu (and to a lesser extent Zn) concentrations are the highest when compared to other industrialized cities of Chile (Tume et al. 2019, 2018a, b, 2018c), China (Lee et al. 2006; Li et al. 2013), or Portugal (Cachada et al. 2013), suggesting that Cu mining emitted significant amounts of these metals.

Elements showing mostly a geogenic signature, such as Co and Cr, exhibited lower concentrations in Tocopilla when compared to soils of southern Chile (e.g., Talcahuano; Tume et al. 2018a) where more basaltic rocks are found along the coastal areas (Western Metamorphic Series; Hervé et al. 2017). Similarly to Athens, Greece, the presence of

Table 8 Published data of median concentrations of trace metals in superficial urban soils of different cities around the world

City (Country)	<i>n</i>	Cr mg/kg	Co mg/kg	Ni mg/kg	Cu mg/kg	Zn mg/kg	Pb mg/kg	Instrument	References
Bangkok (Thailand)	30	25.4	–	23.0	26.6	38	28.9	AAS	Wilcke et al. (1998)
Oslo (Norway)	300	28.5	9.74	24.1	23.5	130	33.9	ICP-AES	Tjihuis et al. (2002)
Palermo (Italy)	70	34	5.2	17.9	64	138	205	GF-AAS	Manta et al. (2002)
Naples (Italy)	173	8.4	–	–	54	180	184	AAS	Imperato et al. (2003)
Hong Kong (China)	236	16.8	3.33	3.65	10.4	78.1	70.6	ICP-AES	Lee et al. (2006)
Galway (Ireland)	166	35	6	22	27	85	58	ICP-AES	Zhang (2006)
Baltimore (United States)	122	38.3	12.1	18.4	35.2	80.7	89.3	ICP-AES	Yesilonis et al. (2008)
Lisbon (Portugal)	51	16	6.8	20	29	88	62	ICP-MS	Cachada et al. (2013)
Viseu (Portugal)	14	10	5.9	4.5	27	80	46	ICP-MS	Cachada et al. (2013)
Shenyang (China)	93	65.10	–	–	71.10	182.00	70.10	ICP-AES	Li et al. (2013)
Athens (Greece)	238	141	16	102	39	98	45	ICP-MS	Argyrazi and Kelepertzis (2014)
Dublin (Ireland)	1058	44.3	9.58	41	35	172	73.7	ICP-AES	Glennon et al. (2014)
Talcahuano (Chile)	140	134	85.9	52.6	–	–	–	P-AAS	Tume et al. (2018a)
Talcahuano (Chile)	140	–	–	–	23.4	60.1	12.5	P-AAS	Tume et al. (2018b)
Arica (Chile)	400	5.6	–	4.7	17	130	112	ICP-OES	Tume et al. (2018c)
Hualpén (Chile)	51	15.0	15.0	33.0	24.0	59.0	6.0	ICP-AES	Tume et al. (2019)
Salerno (Italy)	151	17.2	8	15.3	60.6	129	66.9	ICP-AES	Cicchella et al. (2020)
Tocopilla (Chile, 2014)	60	25	8.1	18	945	305	10	ICP-OES	This study
Tocopilla (Chile, 2020)	18	32	10	18	823	196	27	ICP-OES	This study

All concentrations in mg/kg

serpentinized ophiolitic outcrops were classified as a source of these metals (Argyaki and Kelepertzis 2014 and references therein).

Conclusions

The main conclusions of this research include the following:

- Studied soils of Tocopilla present metals such as Co, Cr, and to a lesser extent Ni, which are mostly related to geogenic sources. On the contrary, Pb, Zn, and Cu are significantly sourced from anthropogenic contributions.
- The weathering of mineral deposits of the Coastal Cordillera is believed to represent the main source of geogenic sourced elements.
- Historic and current mining activities might be related to the highest concentrations of Cu, Zn, and Pb. In addition, thermoelectric plant residues and wind transport might be related to Ni enrichment and to a lesser degree Pb contamination.
- Only Zn and Pb have increased their concentration between the 2014 and 2020 sampling campaigns.
- The urban soils of Tocopilla present the highest concentrations of Cu (and to a lesser extent Zn) when compared to industrial, touristic, and densely populated cities worldwide.

The results of this research are concerning to the population of Tocopilla, which is chronically exposed to Cu, Zn, Pb, and to a lower degree Ni. In this regard, globally, *environmental sacrifice zones* with this level of contamination should not be designated as inhabitable locations. In particular, to safeguard the health of Tocopilla inhabitants, regulators must exert more control over inorganic contaminant emissions, improve mine closure of abandoned small scale mining operations, and ensure continuous monitoring of particulate matter and soils in this high-risk zone. Future studies should focus on health issues derived from the anthropogenic activities present in this city and main redistribution processes controlling metal enrichment and inorganic contaminants.

Supplementary Information The online version contains supplementary material available at <https://doi.org/10.1007/s12665-024-11445-0>.

Acknowledgements This study was partly funded by the National Agency of Research and Development (ANID) of Chile through the Fondecyt Regular grant 1200390 and by an internal grant from Vicerrectoría de Investigación y Desarrollo Tecnológico of Universidad Católica del Norte (Fondo para el desarrollo en investigación científica y tecnológica de actividades de titulación de pregrado y postgrado, 2022). Additional support was provided by Yasna Marambio from the Geochemistry Laboratory of the Earth Sciences Department at UCN; María Ildefonso from CEITSAZA at UCN; Yossie Ossandon from LSA

at UCN; Mario Pereira for support in the field during the 2014 sampling campaigns; Brandon Schneider for English improvement, and Mauricio Medina who supported this research with his ESRI ArcMap 10.8.2 license.

Author contributions Daniela García: conceptualization, methodology, resources, formal analysis, writing—original draft. Joseline Tapia: conceptualization, methodology, resources, writing—original draft. Joaquín Aguilera: formal analysis, methodology, writing—review and editing. Carlos Vega: sampling, writing—review and editing. Pablo Zúñiga: sampling, writing—review and editing. Paris Lavin: writing—review and editing. Luis Rojas: formal analysis, writing—review and editing. Jorge Valdés: resources, writing—review and editing.

Funding Agencia Nacional de Investigación y Desarrollo, Fondecyt Regular 1200390, Universidad Católica del Norte, Fondo para el desarrollo en investigación científica y tecnológica de actividades de titulación de pregrado y postgrado, 2022.

Data availability The data is available in Supplementary Material 1. A phrase similar to the following can be added: All the data obtained for this publication is available in Supplementary Material 1.

Declarations

Conflict of interest The authors declare that there are no competing interests.

Open Access This article is licensed under a Creative Commons Attribution 4.0 International License, which permits use, sharing, adaptation, distribution and reproduction in any medium or format, as long as you give appropriate credit to the original author(s) and the source, provide a link to the Creative Commons licence, and indicate if changes were made. The images or other third party material in this article are included in the article's Creative Commons licence, unless indicated otherwise in a credit line to the material. If material is not included in the article's Creative Commons licence and your intended use is not permitted by statutory regulation or exceeds the permitted use, you will need to obtain permission directly from the copyright holder. To view a copy of this licence, visit <http://creativecommons.org/licenses/by/4.0/>.

References

- Aggarwal CC (2017) An Introduction to outlier analysis. In: Aggarwal CC (ed) Outlier analysis. Springer, Cham, pp 1–34. https://doi.org/10.1007/978-3-319-47578-3_1
- Aguas Antofagasta and GHD (2015) Declaración de Impacto Ambiental Planta Desaladora Tocopilla
- Alcalde J, Kelm U, Vergara D (2018) Historical assessment of metal recovery potential from old mine tailings: a study case for porphyry copper tailings, Chile. *Miner Eng* 127:334–338. <https://doi.org/10.1016/j.mineng.2018.04.022>
- Algoritmos (2019) Campaña de monitoreo de calidad de aire y meteorología estación super site Localidad Tocopilla (Monitoreo No. Informe de Resultados N° 123 MCA036-A1–15). Tocopilla
- Alloway BJ (2013) Sources of heavy metals and metalloids in soils. In: Alloway BJ (ed) Heavy metals in soils: trace metals and metalloids in soils and their bioavailability, environmental pollution. Springer, Netherlands, Dordrecht, pp 11–50. https://doi.org/10.1007/978-94-007-4470-7_2
- Álvarez-Ayuso E, Querol X, Tomás A (2006) Environmental impact of a coal combustion-desulphurisation plant: Abatement capacity of

- desulphurisation process and environmental characterisation of combustion by-products. *Chemosphere, Environ Chem* 65:2009–2017. <https://doi.org/10.1016/j.chemosphere.2006.06.070>
- Anderson T (2003) An introduction to multivariate statistical analysis, Third. Wiley, USA
- Aprisal B, Taufika O, Nurhamidah, (2019) A study of the quality of soil infiltration at the downstream of Kuranji River, Padang City. *GEOMATE J* 16(56):16–20
- Argyriaki A, Kelepertzis E (2014) Urban soil geochemistry in Athens, Greece: the importance of local geology in controlling the distribution of potentially harmful trace elements. *Sci Total Environ* 482–483:366–377. <https://doi.org/10.1016/j.scitotenv.2014.02.133>
- BCN (2007) Declara Zona Saturada por Material Particulado Respirable MP10, como Concentración Anual, a la zona circundante a la ciudad de Tocopilla, Decreto Supremo 50
- BCN (2010) Establece plan de descontaminación atmosférico para la ciudad de Tocopilla y su zona circundante, Decreto Supremo
- BCN (2020) Reportes Estadísticos 2017 de Tocopilla Biblioteca del Congreso Nacional de Chile. https://www.bcn.cl/siit/reportescosmunales/comunas_v.html?anno=2017&idcom=2301. Accessed 2 Aug 2022
- Beck HE, Zimmermann NE, McVicar TR, Vergopolan N, Berg A, Wood EF (2018) Present and future Köppen-Geiger climate classification maps at 1-km resolution. *Sci Data* 5:180214. <https://doi.org/10.1038/sdata.2018.214>
- Bern CR, Walton-Day K, Naftz DL (2019) Improved enrichment factor calculations through principal component analysis: examples from soils near breccia pipe uranium mines, Arizona, USA. *Environ Pollut* 248:90–100. <https://doi.org/10.1016/j.envpol.2019.01.122>
- Bhuiyan MAH, Parvez L, Islam MA, Dampare SB, Suzuki S (2010) Heavy metal pollution of coal mine-affected agricultural soils in the northern part of Bangladesh. *J Hazard Mater* 173:384–392. <https://doi.org/10.1016/j.jhazmat.2009.08.085>
- Cachada A, Dias AC, Pato P, Mieiro C, Rocha-Santos T, Pereira ME, Ferreira da Silva E, Duarte AC (2013) Major inputs and mobility of potentially toxic elements contamination in urban areas. *Environ Monit Assess* 185:279–294. <https://doi.org/10.1007/s10661-012-2553-9>
- Carneiro JR, Almeida PJ, Lopes ML (2018) Laboratory evaluation of interactions in the degradation of a polypropylene geotextile in marine environments. *Adv Mater Sci Eng* 2018:e9182658. <https://doi.org/10.1155/2018/9182658>
- Chen C-W, Kao C-M, Chen C-F, Dong C-D (2007) Distribution and accumulation of heavy metals in the sediments of Kaohsiung Harbor, Taiwan. *Chemosphere* 66:1431–1440. <https://doi.org/10.1016/j.chemosphere.2006.09.030>
- Chiprés JA, de la Calleja A, Tellez JJ, Jiménez F, Cruz C, Guerrero EG, Castro J, Monroy MG, Salinas JC (2009) Geochemistry of soils along a transect from Central Mexico to the Pacific Coast: a pilot study for continental-scale geochemical mapping. *Appl Geochem, Geochem Stud North Am Soils: Res Pilot Stud Phase North Am Soil Geochem Landsc Proj* 24:1416–1428. <https://doi.org/10.1016/j.apgeochem.2009.04.012>
- Cicchella D, Zuzolo D, Albanese S, Fedele L, Di Tota I, Guagliardi I, Thiombane M, De Vivo B, Lima A (2020) Urban soil contamination in Salerno (Italy): concentrations and patterns of major, minor, trace and ultra-trace elements in soils. *J Geochem Explor* 213:106519. <https://doi.org/10.1016/j.gexplo.2020.106519>
- Corradini F, Meza F, Calderón R (2017) Trace element content in soil after a sediment-laden flood in northern Chile. *J Soils Sediments* 17:2500–2515. <https://doi.org/10.1007/s11368-017-1687-3>
- Danzer K, Currie L (1998) Guidelines for calibration in analytical chemistry. Part 1: fundamentals and single component calibration. *Pure Appl Chem* 70(4):993–1014
- de Souza ML (2021) ‘Sacrifice zone’: the environment–territory–place of disposable lives. *Commun Dev J* 56:220–243. <https://doi.org/10.1093/cdj/bsaa042>
- Desaules A (2012) Critical evaluation of soil contamination assessment methods for trace metals. *Sci Total Environ* 426:120–131. <https://doi.org/10.1016/j.scitotenv.2012.03.035>
- DGA (1986) Mapa hidrogeológico de Chile
- DICTUC (2006) Análisis de la Calidad del Aire para MP-10 en Tocopilla. Código BIP 30060200–0. Informe Final. 657145 División Ingeniería Química y Bioprocesos - División Ingeniería de Transporte, 232 pp. https://www.dim.uchile.cl/~lgallard/VOCALS/MONITORING/Informe_Final_Calidad_AIRE_PM10_TOCOPILLA.pdf
- Ferrando F (1992) Clasificación hidrodinámica de Chile. *Cuad Investig Geogr* 18–19:57–74. <https://doi.org/10.18172/cig.1003>. (ISSN 0211-6820)
- Galaz-Mandakovic D (2018) Desechos, aluviones y racismo de Estado. El caso de la población Pacífico Norte de Tocopilla (Chile) 2009–2015/Waste, floods, and state racism. The case of the Pacifico Norte, neighborhood of Tocopilla (Chili) 2009–2015. *Revista Rumbos TS. Un espacio crítico para la reflexión en Ciencias Sociales.* pp 97–130
- Galaz-Mandakovic DG-M (2021) La necroeconomía de la generación de electricidad para la minería. El impacto comunitario del uso del petcoke en Tocopilla (Chile, 2000–2015). *Rev Cuhso* 31:212–249. <https://doi.org/10.7770/cuhso-v31n2-art2155>
- Glennon MM, Harris P, Ottesen RT, Scanlon RP, O’Connor PJ (2014) The Dublin SURGE Project: geochemical baseline for heavy metals in topsoils and spatial correlation with historical industry in Dublin, Ireland. *Environ Geochem Health* 36:235–254. <https://doi.org/10.1007/s10653-013-9561-8>
- González G, Niemeyer H (2005) Cartas Antofagasta y Punta Tetas, Región de Antofagasta, Escala 1:100.000. Carta Geológica de Chile, Serie Geología Básica, n°85
- González G, Cembrano J, Carrizo D, Macci A, Schneider H (2003) The link between forearc tectonics and Pliocene-Quaternary deformation of the Coastal Cordillera, northern Chile. *J S Am Earth Sci* 16:321–342. [https://doi.org/10.1016/S0895-9811\(03\)00100-7](https://doi.org/10.1016/S0895-9811(03)00100-7)
- Guiñez M, Valdés J, Castillo A (2015) Contenido de metales en sedimentos y en Emerita analoga (Stimpson, 1857), en bahía Mejillones del Sur, Chile. *Lat Am J Aquat Res* 43:94–106. <https://doi.org/10.3856/vol43-issue1-fulltext-9>
- Herrera C, Custodio E (2014) Origin of waters from coast of Chile, small springs located at the northern in the vicinity of Antofagasta. *Andean Geol* 41:314–341. <https://doi.org/10.5027/andgeoV41n2-a03>
- Herrera C, Gamboa C, Custodio E, Jordan T, Godfrey L, Jódar J, Luque JA, Vargas J, Sáez A (2018) Groundwater origin and recharge in the hyperarid Cordillera de la Costa, Atacama Desert, northern Chile. *Sci Total Environ* 624:114–132. <https://doi.org/10.1016/j.scitotenv.2017.12.134>
- Hervé F, Fuentes FJ, Calderón M, Fanning M, Quezada P, Pankhurst R, Rapela C (2017) Ultramafic rocks in the North Patagonian Andes: is their emplacement associated with the Neogene tectonics of the Liquiñe-Ofqui Fault Zone? *Andean Geol* 44:1–16. <https://doi.org/10.5027/andgeoV44n1-a01>
- Hower JC, Thomas GA, Mardon SM, Trimble AS (2005) Impact of co-combustion of petroleum coke and coal on fly ash quality: case study of a Western Kentucky power plant. *Appl Geochem* 20:1309–1319. <https://doi.org/10.1016/j.apgeochem.2005.02.010>
- Hu Z, Gao S (2008) Upper crustal abundances of trace elements: a revision and update. *Chem Geol* 253:205–221. <https://doi.org/10.1016/j.chemgeo.2008.05.010>

- Ibrahim LAA (2015) Chemical characterization and mobility of metal species in fly ash–water system. *Water Sci* 29:109–122. <https://doi.org/10.1016/j.wsj.2015.10.001>
- Imperato M, Adamo P, Naimo D, Arienzo M, Stanzione D, Violante P (2003) Spatial distribution of heavy metals in urban soils of Naples city (Italy). *Environ Pollut* 124:247–256. [https://doi.org/10.1016/S0269-7491\(02\)00478-5](https://doi.org/10.1016/S0269-7491(02)00478-5)
- Jorquera H (2009) Source apportionment of PM10 and PM2.5 at Tocopilla, Chile (22°05'S, 70°12'W). *Environ Monit Assess* 153:235–251. <https://doi.org/10.1007/s10661-008-0352-0>
- Khalid S, Shahid M, Niazi NK, Murtaza B, Bibi I, Dumat C (2017) A comparison of technologies for remediation of heavy metal contaminated soils. *J Geochem Explor, Remediat Pollut Soils – Part 2* 182:247–268. <https://doi.org/10.1016/j.gexplo.2016.11.021>
- Kottek M, Grieser J, Beck C, Rudolf B, Rubel F (2006) World Map of the Köppen–Geiger climate classification updated. *Meteorol Z* 15:259–263. <https://doi.org/10.1127/0941-2948/2006/0130>
- Lacassie J, Astudillo F, Baeza L, Carrasco F, Castillo P, Espinoza F, Figueroa M, Miralles C, Muñoz N, Ramírez C (2014) Anomalías geoquímicas en el norte grande y norte chico. Presentación Sernageomin <http://sitiohistorico.sernageomin.cl/pdf/presentaciones-geo/Mapa-geoquimico-del-Norte-de-Chile.pdf>
- Langmyhr FJ, Aadalen U (1980) Direct atomic absorption spectrometric determination of copper, nickel and vanadium in coal and petroleum coke. *Anal Chim Acta* 115:365–368. [https://doi.org/10.1016/S0003-2670\(01\)93179-4](https://doi.org/10.1016/S0003-2670(01)93179-4)
- Lee CS, Li X, Shi W, Cheung SC, Thornton I (2006) Metal contamination in urban, suburban, and country park soils of Hong Kong: a study based on GIS and multivariate statistics. *Sci Total Environ* 356:45–61. <https://doi.org/10.1016/j.scitotenv.2005.03.024>
- Li X, Liu L, Wang Y, Luo G, Chen X, Yang X, Hall MHP, Guo R, Wang H, Cui J, He X (2013) Heavy metal contamination of urban soil in an old industrial city (Shenyang) in Northeast China. *Geoderma* 192:50–58. <https://doi.org/10.1016/j.geoderma.2012.08.011>
- Lo JM, Sakamoto H (2005) Comparison of the acid combinations in microwave-assisted digestion of marine sediments for heavy metal analyses. *Anal Sci* 21:1181–1184. <https://doi.org/10.2116/analsci.21.1181>
- López C, Riquelme R, Martínez F, Sanchez C, Mestre A (2018) Zircon U–Pb geochronology of the mesozoic to lower Cenozoic rocks of the Coastal Cordillera in the Antofagasta region (22°30'–23°00' S): Insights to the Andean tectono-magmatic evolution. *J South Am Earth Sci* 87:113–138. <https://doi.org/10.1016/j.jsames.2017.11.005>
- Luebert F, García N, Schulz N (2007) Observaciones sobre la flora y vegetación de los alrededores de Tocopilla (22°S, Chile). *Bol Museo Nac Hist Nat, Chile* 56:27–52
- Manta DS, Angelone M, Bellanca A, Neri R, Sprovieri M (2002) Heavy metals in urban soils: a case study from the city of Palermo (Sicily), Italy. *Sci Total Environ* 300:229–243. [https://doi.org/10.1016/S0048-9697\(02\)00273-5](https://doi.org/10.1016/S0048-9697(02)00273-5)
- McIlwaine R, Doherty R, Cox SF, Cave M (2017) The relationship between historical development and potentially toxic element concentrations in urban soils. *Environ Pollut* 220:1036–1049. <https://doi.org/10.1016/j.envpol.2016.11.040>
- Mishra G, Marzaioli R, Giri K, Pandey S (2019) Soil quality assessment across different stands in tropical moist deciduous forests of Nagaland, India. *J for Res* 30:1479–1485. <https://doi.org/10.1007/s11676-018-0720-8>
- Mörchen R, Lehdorff E, Diaz FA, Moradi G, Bol R, Fuentes B, Klumpp E, Amelung W (2019) Carbon accrual in the Atacama Desert. *Glob Planet Chang* 181:102993. <https://doi.org/10.1016/j.gloplacha.2019.102993>
- Muller G (1979) Schwermetalle in den Sedimenten des Rheins - Veränderungen seit. *Umschau* 79:778–783
- Muñoz P, Villanelo J, Martínez E, Ahumada I, Retamal M, Saez H, Gómez J, Valdez C, Letelier R, Molina G, Martínez N, Leiva C, Valdés W (2014) Redefinición de la clasificación red hidrográfica a nivel Nacional, Chile. <https://doi.org/10.13140/RG.2.2.23856.00002>
- Nolting RF, Ramkema A, Everaarts JM (1999) The geochemistry of Cu, Cd, Zn, Ni and Pb in sediment cores from the continental slope of the Banc d'Arguin (Mauritania). *Cont Shelf Res* 19:665–691. [https://doi.org/10.1016/S0278-4343\(98\)00109-5](https://doi.org/10.1016/S0278-4343(98)00109-5)
- Nowrouzi M, Pourkhabbaz A (2014) Application of geoaccumulation index and enrichment factor for assessing metal contamination in the sediments of Hara Biosphere Reserve, Iran. *Chem Speciat Bioavailab* 26:99–105. <https://doi.org/10.3184/095422914X13951584546986>
- Oliveros V, Morata D, Aguirre L, Feraud G, Fornari M (2007) Jurassic to Early Cretaceous subduction-related magmatism in the Coastal Cordillera of northern Chile (18°30'–24°S): geochemistry and petrogenesis. *Andean Geol* 34:209–232. <https://doi.org/10.4067/S0716-02082007000200003>
- Oyarzo-Miranda C, Latorre N, Meynard A, Rivas J, Bulboa C, Contreras-Porcía L (2020) Coastal pollution from the industrial park Quintero bay of central Chile: effects on abundance, morphology, and development of the kelp *Lessonia spicata* (Phaeophyceae). *PLoS ONE* 15:e0240581. <https://doi.org/10.1371/journal.pone.0240581>
- Pérez PA, Hintelmann H, Lobos G, Bravo MA (2019) Mercury and methylmercury levels in soils associated with coal-fired power plants in central-northern Chile. *Chemosphere* 237:124535. <https://doi.org/10.1016/j.chemosphere.2019.124535>
- Quezada J, Cerda JL, Jensen A (2010) Efectos de la tectónica y el clima en la configuración morfológica del relieve costero del norte de Chile. *Andean Geol* 37:78–109. <https://doi.org/10.4067/S0718-71062010000100004>
- Reimann C, Filzmoser P, Garrett R, Dutter R (2011) Statistical data analysis explained: applied environmental statistics with R. Wiley, NY
- Reyes A, Thiombane M, Panico A, Daniele L, Lima A, Di Bonito M, De Vivo B (2020) Source patterns of potentially toxic elements (PTEs) and mining activity contamination level in soils of Taltal city (northern Chile). *Environ Geochem Health* 42:2573–2594. <https://doi.org/10.1007/s10653-019-00404-5>
- Rodríguez-Oroz D, Vidal R, Fernandez F, Lambert F, Quiero F (2018) Metal concentrations and source identification in Chilean public children's playgrounds. *Environ Monit Assess* 190:703. <https://doi.org/10.1007/s10661-018-7056-x>
- Rogers G, Hawkesworth CJ (1989) A geochemical traverse across the North Chilean Andes: evidence for crust generation from the mantle wedge. *Earth Planet Sci Lett* 91:271–285. [https://doi.org/10.1016/0012-821X\(89\)90003-4](https://doi.org/10.1016/0012-821X(89)90003-4)
- Rubinos DA, Jerez Ó, Forghani G, Edraki M, Kelm U (2021) Geochemical stability of potentially toxic elements in porphyry copper-mine tailings from Chile as linked to ecological and human health risks assessment. *Environ Sci Pollut Res* 28:57499–57529. <https://doi.org/10.1007/s11356-021-12844-7>
- Rubio B, Nombela MA, Vilas F (2000) Geochemistry of major and trace elements in sediments of the Ria de Vigo (NW Spain): an assessment of metal pollution. *Mar Pollut Bull* 40:968–980. [https://doi.org/10.1016/S0025-326X\(00\)00039-4](https://doi.org/10.1016/S0025-326X(00)00039-4)
- Rudnick RL, Gao S (2003) Composition of the continental crust. In: Holland HD, Turekian KK (eds) *Treatise on geochemistry*, vol 3. Pergamon, Oxford, pp 1–64
- Rutllant J, Fuenzalida H, Torres R, Figueroa D (1998) Interacción océano-atmósfera-tierra en la Región de Antofagasta (Chile, 23°S): experimento DICLIMA. *Rev Chil Hist Nat* 71:405–427
- Rutllant JA, Fuenzalida H, Aceituno P (2003) Climate dynamics along the arid northern coast of Chile: the 1997–1998 Dinámica del

- Clima de la Región de Antofagasta (DICLIMA) experiment. *J Geophys Res Atmos.* <https://doi.org/10.1029/2002JD003357>
- Schulz N, Boisier JP, Aceituno P (2012) Climate change along the arid coast of northern Chile. *Int J Climatol* 32:1803–1814. <https://doi.org/10.1002/joc.2395>
- SERNAGEOMIN (2021) Anuario de la Minería de Chile 2020. Servicio Nacional de Geología y Minería
- Sharma AP, Tripathi BD (2008) Magnetic mapping of fly-ash pollution and heavy metals from soil samples around a point source in a dry tropical environment. *Environ Monit Assess* 138:31–39. <https://doi.org/10.1007/s10661-007-9788-x>
- Sillitoe RH (2003) Iron oxide-copper-gold deposits: an Andean view. *Miner Depos* 38:787–812. <https://doi.org/10.1007/s00126-003-0379-7>
- Sillitoe R (2012) Copper provinces. *Soc Econ Geol Publ* 16:1–18
- Smith DB, Cannon WF, Woodruff LG, Solano F, Ellefsen KJ (2014) Geochemical and mineralogical maps for soils of the conterminous United States (US Government No. 2014–1082). USGS
- Soil Survey Staff (1999) Soil Taxonomy: a basic system of soil classification for making and interpreting soil surveys, 2nd edn. The United States Department of Agriculture (USDA), Washington DC
- Spearman C (1961) The proof and measurement of association between two things. In: Jenkins JJ, Paterson DG (eds) Studies in individual differences: the search for intelligence. Appleton-Century-Crofts, East Norwalk. <https://doi.org/10.1037/11491-005>
- Tapia J, Audry S, Townley B, Duprey JL (2012) Geochemical background, baseline and origin of contaminants from sediments in the mining-impacted Altiplano and Eastern Cordillera of Oruro, Bolivia. *Geochem: Explor Environ, Anal* 12:3–20. <https://doi.org/10.1144/1467-7873/10-RA-049>
- Tapia J, Davenport J, Townley B, Dorador C, Schneider B, Tolorza V, von Tümpling W (2018a) Sources, enrichment, and redistribution of As, Cd, Cu, Li, Mo, and Sb in the Northern Atacama Region, Chile: Implications for arid watersheds affected by mining. *J Geochem Explor* 185:33–51. <https://doi.org/10.1016/j.gexplo.2017.10.021>
- Tapia J, Valdés J, Orrego R, Tchernitchin A, Dorador C, Bolados A, Harrod C (2018b) Geologic and anthropogenic sources of contamination in settled dust of a historic mining port city in northern Chile: health risk implications. *PeerJ* 6:e4699. <https://doi.org/10.7717/peerj.4699>
- Tapia J, Rodríguez M, Castillo P, González R, Rodríguez C, Valdés A, Townley B, Fuentes G (2019) Arsenic and copper in Chile and the development of environmental standards. In: Alaniz AJ (ed) Chile environmental history, perspectives and challenges, vol 7. Nova Science Publishers, New York, pp 241–285
- Tchernitchin AN, Lapin N, Molina L, Molina G, Tchernitchin NA, Acevedo C, Alonso P (2006) Human exposure to lead in Chile. Reviews of environmental contamination and toxicology. Springer, New York, NY, pp 93–139
- Tijhuis L, Brattli B, Sæther OM (2002) A geochemical survey of Topsoil in the City of Oslo, Norway. *Environ Geochem Health* 24:67–94. <https://doi.org/10.1023/A:1013979700212>
- Tume P, González E, King RW, Cuitiño L, Roca N, Bech J (2018a) Distinguishing between natural and anthropogenic sources for potentially toxic elements in urban soils of Talcahuano, Chile. *J Soils Sediments* 18:2335–2349. <https://doi.org/10.1007/s11368-017-1750-0>
- Tume P, González E, King RW, Monsalve V, Roca N, Bech J (2018b) Spatial distribution of potentially harmful elements in urban soils, city of Talcahuano, Chile. *J Geochem Explor Remediat Pollut Soils – Part 3* 184:333–344. <https://doi.org/10.1016/j.gexplo.2016.12.007>
- Tume P, Roca N, Rubio R, King R, Bech J (2018c) An assessment of the potentially hazardous element contamination in urban soils of Arica, Chile. *J Geochem Explor Remediat Pollut Soils – Part 3* 184:345–357. <https://doi.org/10.1016/j.gexplo.2016.09.011>
- Tume P, González E, Reyes F, Fuentes JP, Roca N, Bech J, Medina G (2019) Sources analysis and health risk assessment of trace elements in urban soils of Hualpen, Chile. *CATENA* 175:304–316. <https://doi.org/10.1016/j.catena.2018.12.030>
- Tume P, Acevedo V, Roca N, Ferraro FX, Bech J (2021) Potentially toxic elements concentrations in schoolyard soils in the city of Coronel, Chile. *Environ Geochem Health.* <https://doi.org/10.1007/s10653-021-00909-y>
- Vargas G, Ortlieb L, Rutllant J (2000) Aluviones históricos en Antofagasta y su relación con eventos El Niño/Oscilación del Sur. *Rev Geol Chile* 27:157–176. <https://doi.org/10.4067/S0716-02082000000200002>
- Vargas G, Rutllant J, Ortlieb L (2006) ENSO tropical–extratropical climate teleconnections and mechanisms for Holocene debris flows along the hyperarid coast of western South America (17°–24°S). *Earth Planet Sci Lett* 249:467–483. <https://doi.org/10.1016/j.epsl.2006.07.022>
- Vega AS, Arce G, Rivera JJ, Acevedo SE, Reyes-Paecke S, Bonilla CA, Pastén P (2022) A comparative study of soil metal concentrations in Chilean urban parks using four pollution indexes. *Appl Geochem* 141:105230. <https://doi.org/10.1016/j.apgeochem.2022.105230>
- VID, CITRID (2020) Los territorios que habita(re)mos: ¿qué futuro existe para las zonas de sacrificio? Universidad de Chile. <https://doi.org/10.34720/z5ew-4395>
- Viviani P, Leiva C, Ojeda MJ, Ahumada E, Cortés S (2021) Daños de salud respiratoria en comunas expuestas a centrales termoeléctricas a carbón en el norte de Chile: análisis de datos secundarios. *Rev Chil Enferm Respir* 37:17–25. <https://doi.org/10.4067/S0717-73482021000100017>
- Vural A, Cicek B (2022) Evaluation of Gumustug Antimonite (Torul, Gumushane/Turkiye) mineralization with soil geochemistry and multivariate geostatistical studies. *J Eng Res Appl Sci* 11:2156–2170
- Wang Q-Y, Zhou D-M, Cang L (2014) Bioavailability of soil copper from different sources: integrating chemical approaches with biological indicators. *Pedosphere* 24:145–152. [https://doi.org/10.1016/S1002-0160\(13\)60089-2](https://doi.org/10.1016/S1002-0160(13)60089-2)
- Wilcke W, Müller S, Kanchanakool N, Zech W (1998) Urban soil contamination in Bangkok: heavy metal and aluminium partitioning in topsoils. *Geoderma* 86:211–228. [https://doi.org/10.1016/S0016-7061\(98\)00045-7](https://doi.org/10.1016/S0016-7061(98)00045-7)
- Williams RBG (1986) Intermediate statistics for geographers and earth scientists. Macmillan International Higher Education, London
- Yesilonis ID, Pouyat RV, Neerchal NK (2008) Spatial distribution of metals in soils in Baltimore, Maryland: role of native parent material, proximity to major roads, housing age and screening guidelines. *Environ Pollut* 156:723–731. <https://doi.org/10.1016/j.envpol.2008.06.010>
- Zambra J, Kojima S, Espinoza S, Definis A (2007) Angélica copper deposit: exotic type mineralization in the Tocopilla Plutonic complex of the Coastal Cordillera, Northern Chile. *Resour Geol* 57:427–434. <https://doi.org/10.1111/j.1751-3928.2007.00036.x>
- Zhai X, Li Z, Huang B, Luo N, Huang M, Zhang Q, Zeng G (2018) Remediation of multiple heavy metal-contaminated soil through the combination of soil washing and in situ immobilization. *Sci Total Environ* 635:92–99. <https://doi.org/10.1016/j.scitotenv.2018.04.119>
- Zhang C (2006) Using multivariate analyses and GIS to identify pollutants and their spatial patterns in urban soils in Galway,

- Ireland. *Environ Pollut* 142:501–511. <https://doi.org/10.1016/j.envpol.2005.10.028>
- Zhang Y, Shi T, Yu T, Zhang Y (2013) Sediment particle size and the distribution of heavy metals in the typical districts of Dianchi Lake. *Res Environ Sci* 26:370–379
- Zhu Y, Wang L, Zhao X, Lian J, Zhang Z (2020) Accumulation and potential sources of heavy metals in soils of the Hetao area, Inner Mongolia, China. *Pedosphere* 30:244–252. [https://doi.org/10.1016/S1002-0160\(17\)60306-0](https://doi.org/10.1016/S1002-0160(17)60306-0)
- Zimmerman DW, Williams RH (1997) Properties of the Spearman correction for attenuation for normal and realistic non-normal distributions. *Appl Psychol Meas* 21:253–270. <https://doi.org/10.1177/01466216970213005>
- Zoller WH, Gladney ES, Duce RA (1974) Atmospheric concentrations and sources of trace metals at the south pole. *Science* 183:198–200. <https://doi.org/10.1126/science.183.4121.198>

Publisher's Note Springer Nature remains neutral with regard to jurisdictional claims in published maps and institutional affiliations.